

Cosmogenic ^3He chronology of postglacial lava flows at Mt. Ruapehu, Aotearoa New Zealand

Pedro Doll¹, Shaun Robert Eaves^{2,3}, Ben Matthew Kennedy¹, Pierre-Henri Blard⁴, Alexander Robert Lee Nichols¹, Graham Sloan Leonard⁵, Dougal Bruce Townsend⁵, Jim William Cole¹, Chris Edward Conway⁶, Sacha Baldwin^{1,*}, Gabriel Fénisse^{4,*}, Laurent Zimmermann^{4,*}, and Bouchaïb Tibari^{4,*}

¹School of Earth and Environment, University of Canterbury, Private bag 4800, Christchurch 8041, New Zealand

²Antarctic Research Centre, Victoria University of Wellington, PO Box 600, Wellington 6140, New Zealand

³School of Geography, Environment and Earth Sciences, Victoria University of Wellington, PO Box 600, Wellington 6140, New Zealand

⁴CRPG-CNRS, Université de Lorraine, 15 Rue Notre Dame des Pauvres, Vandoeuvre-les Nancy 54000, France

⁵GNS Science, 1 Fairway Drive, Avalon, Lower Hutt 5011, New Zealand

⁶Geological Survey of Japan, National Institute of Advanced Industrial Science and Technology (AIST), 1-1-1 Higashi, Tsukuba, Ibaraki 305-8567, Japan

*These authors contributed equally to this work.

Correspondence: Pedro Doll (pedro.doll@pg.canterbury.ac.nz)

Abstract. Accurate volcanic hazard assessments rely on a detailed understanding of the timing of past eruptions. While radiometric methods like $^{40}\text{Ar}/^{39}\text{Ar}$ or K/Ar are by far the most conventional lava flow dating tools, their low resolution for young (<20 ka) deposits interferes with the development of precise chronologies of recent effusive activity on most volcanoes. Mt. Ruapehu (Aotearoa New Zealand) has produced many lava flows throughout its history, but the precise timing of many recent eruptions remains largely unknown. In this study, we use cosmogenic ^3He exposure dating to provide 23 eruption ages of young lava flows at Ruapehu. We then compare our results with existing $^{40}\text{Ar}/^{39}\text{Ar}$ and paleomagnetic constraints, highlighting the value of cosmogenic nuclides exposure dating in refining recent eruptive chronologies. Of the 23 sampled flows, 16 provided robust eruption ages (5–20% internal 2σ ; $n \geq 3$) between *ca* 20 and 8 ka, except for one lava erupted at around 43 ka, and their age distribution indicates that, during the last 20 kyr, effusive activity at Ruapehu peaked at 17–12 ka and at 9–7.5 ka. Nearly identical eruption ages of lavas located in different flanks of the volcanic edifice suggest concurrent activity from multiple vents during relatively short time intervals (0–2 kyr) at around 13, 10 and 8 ka. We analysed four individual lava flows previously dated by $^{40}\text{Ar}/^{39}\text{Ar}$, two of which yield eruption ages older than the older limit of the 2σ interval of the radiometric dates, but the good clustering of individual samples from our sites suggests that our results better represent the real eruption age of these flows. Our ^3He -based chronology show excellent agreement with paleomagnetic constraints, suggesting that production rate uncertainties are unlikely to impact the accuracy of our eruption ages. This study demonstrates how cosmogenic nuclides dating can provide greater detail on the recent effusive chronology of statovolcanoes, helping to resolve the low resolution and difficulty in applying radiometric dating methods to young lava flows.

1 Introduction

Effusive volcanism is the main mechanism driving edifice growth on stratovolcanoes and poses a great hazard to infrastructure, the natural environment, and social fabric and livelihoods of local communities (Trusdell, 1995; Wilson et al., 2014; Harris, 2015; Jenkins et al., 2017; Tsang and Lindsay, 2020). Accurate hazard assessments rely on precise knowledge of recent eruption footprints, magnitudes and frequencies (Connor et al., 2015), and hence accurate dating of eruptive events.

Most chronological studies of lava flows on stratovolcanoes are based on radiometric methods, such as $^{40}\text{Ar}/^{39}\text{Ar}$ and K/Ar. Recent advances in these methods (Coble et al., 2011; Fleck et al., 2014; Clay et al., 2015) have improved the precision of age determinations for Pleistocene lavas. However, errors on ages of young (<20 ka) products are still too large to precisely resolve recent eruptive chronologies (e.g., Wijbrans et al., 2011; Conway et al., 2016; Ramos et al., 2016; Calvert et al., 2018; Preece et al., 2018; Pure et al., 2020), hindering our ability to discriminate distinct eruptive episodes or to determine temporal relationships between effusive eruptions and other volcanic processes. If available, radiocarbon dating of burned coal beneath lava flows can provide accurate eruption ages, and has been used widely in Hawai'i (e.g., Buchanan-Banks et al., 1989; Trusdell, 1995, see also Lockwood and Lipman, 1980), as well as in various volcanic regions (e.g., Moore and Rubin, 1991; Mishra et al., 2019; Sherrod et al., 2006). However, the use of radiocarbon is limited to areas with sufficient vegetation at the time of lava flow emplacement, so it is not applicable at high elevations or in periglacial environments. Alternative methods such as paleomagnetism or cosmogenic nuclides exposure dating can support radiometric studies in non-vegetated areas and considerably reduce $^{40}\text{Ar}/^{39}\text{Ar}$ and K/Ar uncertainties for late Pleistocene and Holocene products (Sherrod et al., 2006; Parmelee et al., 2015; Wright et al., 2015; Greve et al., 2016), and are therefore important to generating more accurate eruptive histories in a wider spectrum of volcanic environments.

Cosmogenic nuclides are isotopes that originate when primary and secondary cosmic rays interact with atomic nuclei (Leya et al., 2000; Dunai, 2010). Some of them (terrestrial *in-situ* cosmogenic nuclides, or TCNs) are formed in the upper few metres of the Earth's surface and can be used to calculate exposure ages of geological deposits provided they are: rare in geological materials; produced and retained in common minerals; able to be analysed with reasonable confidence; stable or have a half-life comparable to the timescales of the studied process; and have a well-understood origin and the relative contributions of its production mechanisms are known (Dunai, 2010). The number of TCNs that fulfil these requirements and have well-established methodologies developed for Earth science applications is relatively small (see Dunai, 2010), and the production rates and retention efficiency of TCNs vary across different minerals. ^3He is a stable isotope with the highest production rate of all TCNs and a low detection limit in several geological settings (Blard, 2021), which makes it the ideal nuclide for dating young lava flows (Gosse and Phillips, 2001). This gas suffers diffusion loss in felsic minerals (e.g. quartz and feldspars, and in volcanic groundmass containing them, Lippolt and Weigel, 1988; Tremblay et al., 2014) at Earth's surface temperatures, and is therefore not normally used for silicic lithologies which are better studied using ^{10}Be or ^{26}Al (e.g., Klein et al., 1986; Nishiizumi et al., 1991; Smith et al., 2005). ^3He is more efficiently retained in olivines and pyroxenes (Kurz, 1986a; Gosse and Phillips, 2001; Shuster et al., 2004; Blard, 2021), so it is suitable for dating volcanic eruptions (e.g., Kurz et al., 1990; Foeken et al., 2009; Parmelee et al., 2015), reconstruct glacial histories (e.g., Cerling and Craig, 1994; Blard et al., 2007) and fault

kinematics (e.g., Fenton et al., 2001) or estimate erosion rates (e.g., Ferrier et al., 2013; Puchol et al., 2017), considering that the studied rocks contain these minerals.

Surface exposure dating using TCNs is applicable to geological deposits that have been brought to the surface and remained exposed to the cosmic ray flux ever since, provided there is no significant erosion or shielding (glacial, snow, debris, soil, tephra, or vegetation cover) which could have affected their cosmogenic nuclide inventory. In temperate climates, suitable sites will lie at elevations between the vegetation limit and where cryogenic processes begin to dominate. In dynamic environments such as stratovolcanoes, original surfaces are more likely to be preserved on younger lava flows, which have had a relatively limited time exposed to erosive and/or depositional processes. In addition, flow interiors with crystalline groundmass necessary for $^{40}\text{Ar}/^{39}\text{Ar}$ or K/Ar dating are less likely to be exposed in young lava flows for the same reason. For young lava flows, cosmogenic ^3He ($^3\text{He}_{\text{cos}}$) has the potential to resolve events down to 100 years under the most favourable conditions (low magmatic He and eruption ages ≤ 10 ka; Niedermann, 2002) and commonly yields ages with uncertainties of 15–20% (2σ including production rate errors), significantly more precise than traditional radiometric techniques for lavas < 20 ka (e.g., Wijbrans et al., 2011; Calvert et al., 2018; Pure et al., 2020). Thus, $^3\text{He}_{\text{cos}}$ can be used to complement chronological studies by providing greater detail on recent construction histories of volcanic edifices (e.g., Kurz et al., 1990; Foeken et al., 2009; Espanon et al., 2014; Parmelee et al., 2015). However, most of this research is focused on basaltic lava flows in extensional environments (e.g., Kurz et al., 1990; Licciardi et al., 2007; Foeken et al., 2009; Espanon et al., 2014; Marchetti et al., 2014; Medynski et al., 2015), and the application of $^3\text{He}_{\text{cos}}$ on stratovolcanoes (e.g., Parmelee et al., 2015) is still limited. 'A'ā lavas (commonly found in andesitic stratovolcanoes) have normally prominent tumuli standing out from the landscape, which are less likely to accumulate large amounts of snow or tephra compared to flatter primary morphologies (e.g. ropy pāhoehoe surfaces targeted in basic lavas, Kurz et al., 1990; Espanon et al., 2014; Marchetti et al., 2014; Parmelee et al., 2015), making them ideal targets for surface exposure dating (see Licciardi et al., 2007).

In this paper, we use surface exposure dating with terrestrial *in-situ* $^3\text{He}_{\text{cos}}$ in pyroxenes and olivines to provide 23 eruption ages of mainly postglacial (< 20 ka) lava flows at Mt. Ruapehu, a large (summit 2797 m asl) andesitic stratovolcano located in the centre of Te Ika-a-Māui (North Island of Aotearoa New Zealand). We then compare our results with previous $^{40}\text{Ar}/^{39}\text{Ar}$ and paleomagnetically-refined ages, as well as with eruption age assumptions based on geochemical fingerprinting, and test the applicability of $^3\text{He}_{\text{cos}}$ as a lava flow dating tool for stratovolcanoes, showcasing the method's capacity to provide high resolution ages for young lava flows and to identify distinct eruptive episodes in short time intervals.

2 Geological background

2.1 Study area

Ruapehu is a cultural and spiritually significant *Maunga* (Māori word for mountain) for local Iwi (Māori tribes) Ngāti Rangi, Ngāti Tūwharetoa and Uenuku (see Gabrielsen et al., 2018). This volcano is the southernmost continental expression of the Taupō Volcanic Zone (TVZ, Figure 1), related to the Hikurangi Trench, the southern end of the Tonga-Kermadec arc subduction system (Cole and Lewis, 1981). The TVZ can be divided into three segments: the northern, central and southern TVZ

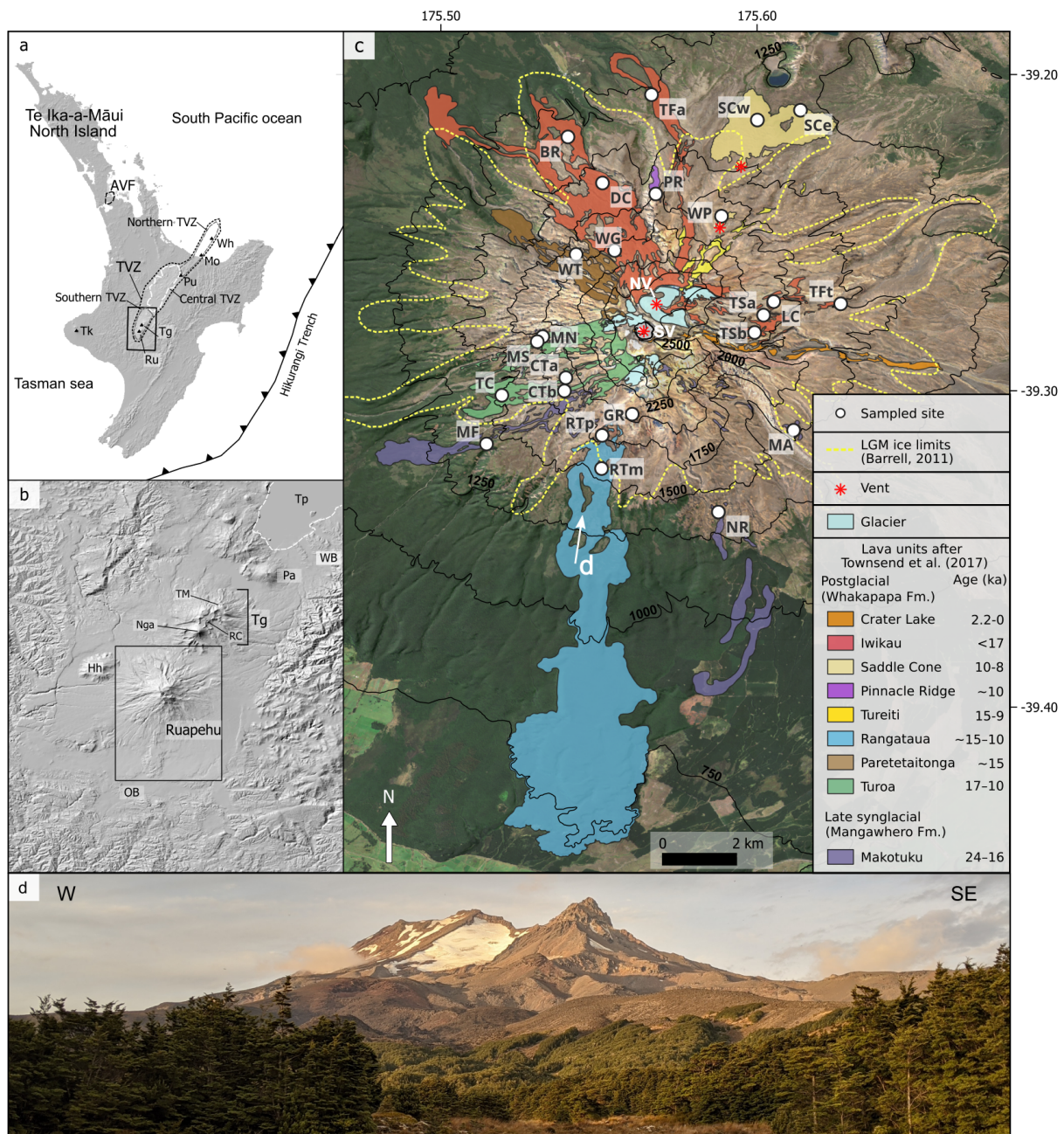


Figure 1. Location map of study area. a) Te Ika-a-Māui (North Island of Aotearoa New Zealand) with its main active volcanic areas detailed. (AVF) monogenetic Auckland Volcanic Field; (Wh) Whakaari-White Island; (Mo) Motuhara; (Pu) Putauaki; (TVZ) Taupō Volcanic Zone; (Tg) Tongariro; (Ru) Ruapehu; (Tk) Taranaki. b) Detail of the "Central Plateau", at the southern end of the TVZ. (Tp) Taupō; (WB) Waimarino Basalt; Pihanga (Pa); (Tg) Tongariro; (TM) Te Maari; (Nga) Ngauruhoe; (RC) Red Crater; (Hh) Hauhungutahi; (OB) Ohakune Formation basalt. c) Study area, with Ruapehu's postglacial and late synglacial lava units mapped after Townsend et al. (2017) and sampled sites in this study. Maximum glacial extent during the LGM (last glacial maximum, ~20–15 ka) after Barrell (2011) outlined with black dashed line. (NV) Northern vent; (SV) Southern Vent. Abbreviations next to sampled sites refer to lava flow names, full list in Table A1. d) Photo of Ruapehu taken from the south, with Mangaehuehu Glacier directly beneath Ruapehu's summit (viewpoint's location is shown in (c) with the white arrow labelled (d)).

(Figure 1a), distinguished by composition and eruptive styles. The northern TVZ has several andesitic stratovolcanoes, including Whakaari-White Island and Motuhara off the northeastern coast of Te Ika-a-Māui North Island. The central TVZ is one of the most productive silicic volcanic systems in the world, with at least 34 caldera-forming events in the last 1.6 Ma, including Taupō and Ōkataina (Houghton et al., 1995; Wilson et al., 2009). The southern zone is dominated by the andesitic stratovolcanoes Tongariro and Ruapehu, with subordinate basalts (e.g. Ohakune Formation basalt).

Ruapehu is the largest and one of the most active stratovolcanoes in mainland Aotearoa New Zealand (Leonard et al., 2021). The current edifice is mostly formed by pyroxene-bearing basaltic andesite, andesite, and dacite lavas, which erupted throughout four main constructive periods, and are encompassed in distinct units; Te Herenga (200–150 ka), Waihianoa (150–80 ka), Mangawhero (50–15 ka) and Whakapapa (15–2 ka) formations (Hackett, 1985; Townsend et al., 2017). Contemporary to lava flow emplacement, Ruapehu generated many explosive eruptions (Topping and Kohn, 1973; Donoghue et al., 1995; Pardo et al., 2012a), including several plinian events (Pardo, 2012) preserved as tephra sequences on the eastern volcanic ring plain, although the timing of these eruptions is not well constrained. In this study, we focus on the Whakapapa Formation and the youngest member of the Mangawhero Formation (Figure 1; Table 1), providing greater detail on the recent effusive activity of Ruapehu.

Eruption ages of Ruapehu’s lava flows were first determined using K/Ar (Stipp, 1968; Tanaka et al., 1997) and later improved with $^{40}\text{Ar}/^{39}\text{Ar}$ by Gamble et al. (2003) and Conway et al. (2016). Combining these $^{40}\text{Ar}/^{39}\text{Ar}$ ages with an extensive geochemical survey, Conway et al. (2016) divided lavas from the Mangawhero and Whakapapa formations into distinctive packages, later formalized as members by Townsend et al. (2017, Table 1). However, many lava flows are only assumed to have been erupted in specific time periods due to their geochemical similarity and/or geographical proximity to flows with geochronological constraints.

Throughout its history, Ruapehu has periodically been covered by glaciers controlling lava flow emplacement (Conway et al., 2015). The edifice displays characteristic erosional and depositional glacial landforms extending from current glaciers down to ~1200 m asl (Mc Arthur and Shepherd, 1990; Eaves et al., 2016a; Townsend et al., 2017) and conspicuous large and fine-scale features indicative of lava-ice interaction. During heavily glaciated periods, lava emplacement and preservation were restricted to inter-valley ridges, and cooling against ice generated overthickened lava margins (ice-bounded flows; Conway et al., 2015) still visible in the landscape. Based on the distribution of these ice-bounded lava flows, Conway et al. (2016) suggested a peak in glacial expansion between 42 and 31 ka and a reduction in ice thickness between 31 ka and the last stages of the last glacial maximum (LGM) at 20–15 ka (Barrell et al., 2013), prior to the glacial retreat. Effusive deposits erupted after the LGM (postglacial lavas of the Whakapapa Formation, Figure 1) were free to flow to the valley floors and finished shaping the modern landscape observed at Ruapehu. Eaves et al. (2019) provided $^3\text{He}_{\text{cos}}$ ages for moraine groups on the Mangaehuehu valley (south Ruapehu) recording pulsatory glacial retreat after the LGM. Based on $^3\text{He}_{\text{cos}}$ exposure ages of boulders, they proposed moraine construction periods and associated equilibrium line altitudes of 2100 m asl at ~14–11 ka, 2250 m asl at 4.5 ka, and 2300 m asl at 200–500 yr ago. Present glaciers on Ruapehu (3.0 km² on 2016; Eaves and Brook, 2021) are restricted to some upper catchment areas over 2250 m asl, the largest of which is located on its summit plateau at >2500 m asl.

Formation	Member		Eruption ages ($\pm 2\sigma$)	Methods	^3He -based eruption ages, this study (ka, $\pm 2\sigma$)
Whakapapa (<15 ka; postglacial)	Crater Lake (<5 ka)		2400–2050 BP ⁽¹⁾ , 0.2 ± 2.2 ka ⁽²⁾	Paleomagnetism (refined from $^{40}\text{Ar}/^{39}\text{Ar}$)	-
	Iwikau	Tawhainui flows (9–7 ka)	DC: 8200–7900 BP ⁽¹⁾ , 6.0 ± 2.4 ka ⁽²⁾ ; BR: 8800–8500 BP ⁽¹⁾	Paleomagnetism (refined from $^{40}\text{Ar}/^{39}\text{Ar}$ and tephra stratigraphy)	DC: 7.8 ± 1.5 ; BR: 8.1 ± 2.1 ; WG: $\geq 7.8 \pm 2.4$
		Mangatoetoenui flows (<17 ka*)	LC: 0.8 ± 5.6 ka; TSb: 9.2 ± 8.0 ka ⁽²⁾	$^{40}\text{Ar}/^{39}\text{Ar}$	LC: 11.4 ± 2.3 ; TSa: 9.4 ± 1.8 ; TSb: 11.5 ± 2.2 ; TFt: $\geq 8.6 \pm 2.6$
		Taranaki Falls flow (11–9 ka*)	TFa: 10 800–8900 BP ⁽¹⁾ , 8.8 ± 2.8 ka ⁽²⁾	Paleomagnetism (refined from $^{40}\text{Ar}/^{39}\text{Ar}$)	TFa: 14.6 ± 2.9
	Saddle Cone (10–8 ka*)		SC: 9850–8650 BP ⁽¹⁾	Paleomagnetism (refined from tephra stratigraphy)	SC: 9.9 ± 2.0 ; WP: $\geq 11.2 \pm 2.2$
	Pinnacle Ridge (~ 10 ka*)		PR: ~ 10 ka ⁽³⁾	Correlation with tephra	PR: 20.4 ± 4.0
	Tureiti (15–9ka)		12.5 ± 2.6 ; 11.9 ± 2.8 ka ⁽²⁾	$^{40}\text{Ar}/^{39}\text{Ar}$	-
	Rangataua (~ 15 –10 ka*)		~ 15 –10 ka ^(4,5)	Stratigraphy	RTp: 13.6 ± 2.6 ; RTm: 15.8 ± 3.0
	Paretetaitonga (~ 15 ka)		14.8 ± 3.0 ka ⁽²⁾	$^{40}\text{Ar}/^{39}\text{Ar}$	WT: 13.3 ± 2.6
	Turoa (17–10 ka*)		15.1 ± 2.4 ; 11.9 ± 2.2 ka ⁽²⁾	$^{40}\text{Ar}/^{39}\text{Ar}$	MN: 8.3 ± 1.6 ; MS: $\geq 6.1 \pm 1.7$; CTa: $\geq 13.6 \pm 2.7$; CTb: 8.6 ± 1.7 ; TC: 13.4 ± 2.6
Mangawhero (50–15 ka; synglacial)	Makotuku (24–16 ka)		20.9 ± 2.8 ; 17.8 ± 2.2 ka ⁽²⁾	$^{40}\text{Ar}/^{39}\text{Ar}$	MF: 12.6 ± 3.5 ; NR: 42.9 ± 8.6 ; MA: $\geq 54.0 \pm 18.0$
	Waitonga (25–21 ka)		$23.0 \pm 1.6^{(2)}$; 23 ± 8 ka ⁽⁶⁾	$^{40}\text{Ar}/^{39}\text{Ar}$	-
	Te Piripiri (~ 21 ka)		21 ± 6 ka ⁽⁶⁾	$^{40}\text{Ar}/^{39}\text{Ar}$	-
	Horonuku (29–15 ka)		23 ± 4 ; 22 ± 7 ka ⁽⁶⁾	$^{40}\text{Ar}/^{39}\text{Ar}$	-
	Whakapapaiti (~ 26 ka)		25.7 ± 3.8 ka ⁽²⁾	$^{40}\text{Ar}/^{39}\text{Ar}$	-
	Manganuioteao (36–22 ka)		25.7 ± 2.6 ; 27.2 ± 4.8 ; 30.7 ± 5.2 ; 30.9 ± 2.2 ka ⁽²⁾	$^{40}\text{Ar}/^{39}\text{Ar}$	-
	Mananui (42–38 ka)		$40.3 \pm 2.2^{(2)}$	$^{40}\text{Ar}/^{39}\text{Ar}$	-
	Te Kohatu (44–36 ka)		47.6 ± 1.4 ; 39.1 ± 1.4 ; 39.2 ± 2.0 ; 42.6 ± 1.8 ka ⁽²⁾	$^{40}\text{Ar}/^{39}\text{Ar}$	-
	Mangaturuturu (46–36 ka)		38.4 ± 2.4 ; 41.3 ± 1.8 ; 43.4 ± 2.4 ka ⁽²⁾	$^{40}\text{Ar}/^{39}\text{Ar}$	-
	Mangaehuehu (47–40 ka)		42.8 ± 1.0 ; 43.1 ± 1.4 ; 43.3 ± 1.6 ; 44.2 ± 1.8 ; 45.4 ± 2.0 ka ⁽²⁾	$^{40}\text{Ar}/^{39}\text{Ar}$	GR: $\geq 14.2 \pm 2.7$
	Ngahuinga (48–35 ka)		44.8 ± 3.0 ka ⁽²⁾	$^{40}\text{Ar}/^{39}\text{Ar}$	-
Waihianoa (166–80 ka)		88.1 ± 6.4 ; 95.9 ± 7.0 ; 120.7 ± 4.0 ; 121.4 ± 2.8 ; 121.7 ± 4.2 ; 133.6 ± 6.4 ⁽²⁾ ; 119 ± 12 ; 129 ± 15 ; 130 ± 23 ; 131 ± 27 ; 133 ± 11 ; 134 ± 12 ; 135 ± 14 ; 138 ± 14 ; 147 ± 10 ; 147 ± 12 ; 154 ± 12 ka ⁽⁶⁾	$^{40}\text{Ar}/^{39}\text{Ar}$	-	
Te Herenga (200–150 ka)		158.8 ± 8.2 ; 169.4 ± 7.8 ; 174.6 ± 3.4 186.2 ± 6.8 ; 187.9 ± 34.4 ⁽²⁾ ; 183 ± 13 ; 197 ± 12 ; 205 ± 27 ka ⁽⁶⁾	$^{40}\text{Ar}/^{39}\text{Ar}$	-	

Table 1. Previous chronological studies from lava flows at Ruapehu: 1) Greve et al. (2016); 2) Conway et al. (2016); 3) Donoghue et al. (1999); 4) Price et al. (2012); 5) Eaves et al. (2016b); 6) Gamble et al. (2003). *Age limits redefined in this study based on $^3\text{He}_{\text{cos}}$ eruption ages. Ages separated by commas represent the same lava flow, semicolons separate dates from different flows.

2.2 Previous chronological studies on postglacial lavas

120 The first constraints on eruption ages of Whakapapa lavas were given from studies of tephra layers (Topping, 1974; Price et al., 2012). Conway et al. (2016) were the first to provide absolute ages using $^{40}\text{Ar}/^{39}\text{Ar}$, for which samples from slowly-cooled lava interiors are needed, as Ar analyses are done in crystalline groundmass (glass contents <5%) with large microlites. The lack of abundant exposures of lava interiors limited its application to only 10 flows, and although this technique yielded reasonably precise ages for lavas >20 ka, their relative errors increase with decreasing age, varying between 16 and 23% for 20–11 ka deposits and 32 and 1000% for Holocene lavas (see Table 1).

Greve et al. (2016) refined the eruption age for $^{40}\text{Ar}/^{39}\text{Ar}$ -dated and tephra-constrained Holocene lava flows by comparing characteristic magnetization directions recorded in the lavas with a paleosecular variation record based on lake sediments from Lake Mavora (Te Waipounamu South Island, Aotearoa New Zealand) independently calibrated using ^{14}C (Turner et al., 2015). Dating lava flows using paleomagnetic directions, however, requires a previous eruption age constraint and is limited to the Holocene in Aotearoa New Zealand due to the extension of the sediment record. Only the ages of five flows were constrained using this method: one from the Crater Lake Member, three from the Iwikau Member (Delta Corner, Bruce Road and Taranaki Falls flows) and the western lobe of the Saddle Cone Member. Eruption ages provided by Greve et al. (2016) for the Crater Lake, Delta Corner and Bruce Road flows are tightly constrained (age ranges of *ca* 300 yrs), while their preferred ages for the Taranaki Falls flow and Saddle Cone Member span over ~2 and ~1.2 kyr, respectively (Table 1).

135 3 Methods

3.1 Sampling site selection

The selection of an adequate sampling site is an important step for cosmogenic nuclides exposure dating. Evidence of negligible erosion is essential, as well as confidence that the targeted rock has not been covered by other rocks, soil, ice, volcanic ash or vegetation for a significant amount of time since formation. For lava flows, effective sampling was achieved by targeting tumuli, spikes and other features standing above the main flow surface (e.g., Anderson et al., 1994; Licciardi et al., 2006) which preserve characteristic primary cooling morphologies of flow surfaces (Figure 2). Additional photos of sampled sites and examples of not suitable sites can be found in the supplementary file S1.

Using aerial photographs and digital elevation models (DEMs) based on aerial imagery and a newly acquired LiDAR dataset, we revised the existing maps (Townsend et al., 2017) and identified individual lava flows within each of the different members of the Whakapapa Formation, which we then targeted in our sampling. Lack of adequate lava surface exposures did not permit us to sample lavas from the Tureiti and Crater Lake members. Due to the lack of chronological data on several lavas of the Makotuku Member of the Mangawhero Formation (24–16 ka; Conway et al., 2016, Table 1), we additionally targeted three flows of this unit on outcrops outside of the LGM ice limits (MF, NR, MA; Figure 1c). We also sampled a site (GR) that we consider to be postglacial due to the presence of original (non-eroded) lava surfaces and its location inside the LGM ice limit of

150 Barrell (2011, Figure 1c). Note that this exposure was previously mapped as Mangawhero Formation (Mangaehuehu Member) based primarily on its location on the volcano and similarity in appearance to nearby geochemically fingerprinted outcrops.

3.2 Sample collection

All samples were collected under a Research and Collection Permit of the Department of Conservation of Aotearoa New Zealand, obtained after a consultation process involving local Iwi (Māori tribes) with rightful claims to guardianship of Ru-
155 apehu. We sampled between three and six shallow surfaces (<6 cm below the flow top) for each targeted flow using a hammer and chisel. For recording the coordinates and altitude of each surface (vertical precision of 0.1 m) we used a differential Trimble Geo7X GPS corrected by data of VGMT (Ohakune, Land Information New Zealand) and the Chateau Observatory Base (GeoNet) stations. We also measured surface dip and orientation and azimuth-horizon angle pairs to account for topographic shielding. For the CTa, CTb and TC samples, *in situ* topographic shielding could not be acquired, so representative azimuth-
160 horizon angle pairs were selected based on observations of DEMs. To test the accuracy of this approach, we compared values derived from DEMs to field-obtained shielding factors from other sites, showing an agreement of 95–99%.

3.3 Mineral separation

For each sample fragment used, mean thickness was calculated using a caliper in 5–40 points, and then a sample thickness average was obtained weighted by rock fragment mass. Afterwards, samples were crushed and sieved to obtain a 100–1000
165 μm size fraction, which was then rinsed to eliminate dust and organic matter and dried at 60° C.

Density separation was done using a 3.0 g/cm³ sodium polytungstate solution, after which the heavy concentrates were leached in a 5% HF; 2.5% NaOH bath for 24 hours before immersing in 3M HCl to remove fluoride precipitates, following Bromley et al. (2014). After checking under a microscope, we leached a second and third time if necessary in 5% HF; 2.5% NaOH and/or 2.5% HF; 1.25% NaOH, until we achieved total removal of groundmass on most crystals. We then carried out
170 magnetic separation of oxides and magnetic groundmass, and finally removed remaining impurities visually, based on colour and texture, to leave pure pyroxenes (olivines and pyroxenes in the GR samples).

3.4 Geochemical analyses

For each studied lava flow, major and trace element compositions were analysed at the Service d'Analyse des Roches et Minéraux (SARM) of the Centre de Recherches Pétrographiques et Géochimiques (CRPG, Université de Lorraine, Nancy,
175 France) by inductively coupled plasma optical emission spectroscopy (ICP-OES) and inductively coupled plasma mass-spectrometry (ICP-MS), respectively, both for bulk rock and pure pyroxenes/olivines. Each analysed sample consisted of 1 g of powdered rock/minerals that were fused at 980 °C for 60 minutes in Pt crucibles together with ultra pure LiBO₂ in a 1:3 ratio prior to glass dissolution and measurements. The complete procedure is described in detail in Carignan et al. (2001).



Figure 2. Examples of targeted sites. Red arrows point to a 20 cm long GPS. a), b), c) and d) represent typical sampled surfaces ('a'ā morphologies). a) Large tumuli, 1.5 m above ground level (sample RTp-PD027). b) Large tumuli, 2.5 m above ground level (sample DC-PD330). c) Detail of lava top. Rough, irregular surfaces resembling 'a'ā lava flow morphologies, indicatives of minimal erosion (sample MN-PD220). d) 'A'ā block standing out ~40 cm above the ground, pencil for scale (sample SC-PD001). e) Surface of the Pinnacle Ridge spatter deposit (sample PR-PD085). f) Sampled surface of the Waihothonu Plateau blocky flow (sample WP-PD008).

3.5 Measurement of Helium isotopes concentrations

180 We analysed ^3He and ^4He concentrations in pyroxenes and olivines using a GV Instruments Helix Split Flight Tube multi-collector noble gas mass spectrometer attached to a gas line at CRPG (e.g., Schimmelpfennig et al., 2011; Blard et al., 2013, 2015).

Pure minerals were wrapped in tin capsules, loaded in a carousel and baked for one night at 100°C under ultrahigh vacuum. The samples were heated to $>1300^\circ\text{C}$ for 15 minutes in a full metal induction furnace (Zimmermann et al., 2018) and gases
185 expelled were purified using four activated charcoal traps at 77 K in order to trap large amounts of CO_2 , H_2O , N_2 and heavy noble gases (Ar, Kr and Xe) from the melted samples by physisorption. In parallel, four getters initially activated at 800°C were used at room temperature to trap all reactive species (e.g. H_2O , CO_2 , N_2 , O_2) by chemisorption. After these two steps, He was condensed using a cryogenic trap at 12 K under ultra-low pressure ($0.5\text{--}1 \times 10^{-8}$ mbar), and then released at 75 K towards the mass spectrometer that measured, in static mode, ^3He and ^4He . The source settings were adjusted to get the best
190 compromise between linearity, sensibility and stability (e.g. ^3He sensitivity = $4.30 \times 10^{18} \pm 5\%$ cps/mol, ^4He sensitivity = $7.45 \times 10^{13} \pm 2\%$ mV/mol). HESJ gas standards (20.63 R/Ra, Matsuda et al., 2002, Ra: atmospheric $^3\text{He}/^4\text{He}$ ratio of 1.39, Lupton and Evans, 2013) were measured daily with a reproducibility of 4.7% and ^4He and ^3He values were also routinely compared with CRONUS-P standards (Blard et al., 2015; Schaefer et al., 2016, reproducibility of 5.0%). The main source of background He (measured daily, typical ^3He blanks $< 5 \pm 3.5 \times 10^3$ atoms; typical ^4He blanks of $1.3 \times 10^9 \pm 1.8 \times 10^8$ atoms; $^3\text{He}/^4\text{He}$
195 ratios similar to 1 Ra) was the Ta crucible, which was degassed at 1800°C for 30 minutes prior to analyses.

Crushed-released He isotopic analyses (used for magmatic corrections) were performed in samples with larger crystals (dominant fraction 500–1000 μm , which were shown to contain larger amounts of magmatic He likely hosted in melt inclusions, Puchol et al., 2017) using a soft iron slug activated by external solenoids. Samples were crushed for 5 to 7 min at 100 strokes/min, with tube-specific ^3He blanks between 3.8 ± 1.1 and $0.6 \pm 0.3 \times 10^4$ atoms, and ^4He blanks between 3.1 ± 0.1
200 $\times 10^9$ and $2.0 \pm 1.8 \times 10^8$ atoms. For a detailed description of the in-vacuo crushing He extraction method see Puchol et al. (2017).

3.6 Surface exposure age determinations

3.6.1 Calculation of cosmogenic ^3He

To correctly determine the concentration of $^3\text{He}_{\text{cos}}$, it is necessary to consider the non-cosmogenic contributions to total ^3He
205 measured when fused in vacuo ($^3\text{He}_{\text{tot}}$), described by the equation:

$$^3He_{\text{tot}} = ^3He_{\text{cos}} + ^3He_{\text{atm}} + ^3He_{\text{nuc}} + ^3He_{\text{mag}} \quad (1)$$

where $^3\text{He}_{\text{atm}}$ is the atmospheric ^3He hosted at the minerals' surfaces as a contaminant and is time independent. $^3\text{He}_{\text{nuc}}$ is the nucleogenic ^3He produced by capture of low-energy neutrons emitted by ^6Li and dependent on Li concentrations in the mineral, U and Th concentrations in the rock, and the mineral closure age (equivalent to eruption age for pyroxenes and

210 olivines in volcanic rocks, Kurz, 1986a). ${}^3\text{He}_{\text{mag}}$ is the magmatic ${}^3\text{He}$ contribution (time independent) present in melt and fluid inclusions, and within the matrix of the minerals.

Atmospheric He (both ${}^3\text{He}$ and ${}^4\text{He}$) concentrations are inversely proportional to the mineral grain size and become insignificant for minerals larger than 100 μm (Blard, 2021), so they were considered non-existent in our calculations. ${}^3\text{He}_{\text{nuc}}$ quotas are normally negligible for uneroded lava flows, in which the closure and exposure ages are the same (Kurz, 1986a), as shown
215 by our calculations (Table A3) based on the spreadsheet developed by Blard (2021).

The total contribution of ${}^3\text{He}_{\text{mag}}$ was accounted for in Equation 3, and estimated using a magmatic ratio obtained as an uncertainty-weighted average from isotopic analyses of three samples crushed in vacuo and previous data from pyroxene and olivine phenocrysts in the Waimarino and Ohakune basalts (subsection 4.2 and supplementary files S2.1 and S2.2).

The total amount of ${}^4\text{He}$ measured in each sample (${}^4\text{He}_{\text{tot}}$) is defined by the equation:

$$220 \quad {}^4He_{\text{tot}} = {}^4He_{\text{mag}} + {}^4He_{\text{atm}} + {}^4He_{\text{rad}} + {}^4He_{\text{cos}} \quad (2)$$

where ${}^4\text{He}_{\text{mag}}$ corresponds to the time independent magmatic ${}^4\text{He}$ quota naturally present in the minerals, while ${}^4\text{He}_{\text{atm}}$ accounts for atmospheric ${}^4\text{He}$ contaminating the minerals' surfaces (time independent). ${}^4\text{He}_{\text{rad}}$ is generated by the decay of radioactive isotopes such as U, Th and Sm present in the minerals and dependent on the abundance of these elements in the minerals, and the closure age. Crystals normally exhibit an enriched ${}^4\text{He}$ exterior rim generated by implanted ${}^4\text{He}_{\text{rad}}$ from
225 the matrix (Lal, 1989), typically with higher concentrations of U, Th and Sm. ${}^4\text{He}_{\text{cos}}$ refers to the cosmogenic contribution of ${}^4\text{He}$, negligible compared to other non-cosmogenic varieties of ${}^4\text{He}$ (Blard, 2021) and are therefore also omitted from our calculations.

In this paper we follow the approach of Blard and Farley (2008), which corrects for the contributions of ${}^4\text{He}_{\text{rad}}$, ${}^4\text{He}_{\text{mag}}$ and ${}^3\text{He}_{\text{mag}}$ for uneroded lava flows, using the equation:

$$230 \quad {}^3He_{\text{cos}} = \frac{{}^3He_{\text{tot}} - {}^4He_{\text{tot}} \left(\frac{{}^3He}{{}^4He} \right)_{\text{mag}}}{R} \quad (3)$$

where R (or R factor) is defined by:

$$R = 1 - \left(\frac{P_4}{P_3} \right) \left(\frac{{}^3He}{{}^4He} \right)_{\text{mag}} \quad (4)$$

where P_4 and P_3 are the ${}^4\text{He}_{\text{rad}}$ and local ${}^3\text{He}_{\text{cos}}$ production rates.

The use of the R factor is essential when using ${}^3\text{He}_{\text{cos}}$ to date uneroded lava flows, as it permits the incorporation of a
235 time-dependant ${}^4\text{He}_{\text{rad}}$ quota, avoiding the issue of under- or overestimation of the ${}^4\text{He}_{\text{mag}}$ (and hence ${}^3\text{He}_{\text{mag}}$) contribution.

Individual values of P_4 were calculated for each lava flow using the spreadsheet developed by Blard (2021), neglecting the implanted ${}^4\text{He}_{\text{rad}}$ component to account for the removal of the ${}^4\text{He}$ -enriched crystal rim with HF leaching.

Sample-specific P_3 estimates were obtained following the Lal-Stone time corrected scaling scheme (Lal, 1991; Stone, 2000; Nishiizumi, 1989; Balco et al., 2008) using the online calculator 'Cosmic Ray Exposure program' (CREp, [https://crep.otelo.
240 univ-lorraine.fr/](https://crep.otelo.univ-lorraine.fr/); Martin et al., 2017) and the global ${}^3\text{He}_{\text{cos}}$ production rate database therein.

3.6.2 Determination of exposure and eruption ages

To obtain exposure ages, we used the CREp online calculator, which calculated exposure ages based on our $^3\text{He}_{\text{cos}}$ concentrations and scaling parameters, Lal-Stone time corrected scaling scheme (Lal, 1991; Stone, 2000; Nishiizumi, 1989; Balco et al., 2008), ERA40 atmosphere model (Uppala et al., 2005), the geomagnetic framework of Muscheler et al. (2005) and worldwide mean $^3\text{He}_{\text{cos}}$ production rates of 122 ± 12 at/g/yr at sea level on high latitudes (SLHL).

Exposure ages calculated using the LSD scaling scheme (Lifton et al., 2014) and different atmospheric models and geomagnetic databases are available in the supplementary material (S3), showing variations of 1–3% compared with the exposure ages calculated using the parameters outlined above. This is, however, not the case of the LSD geomagnetic framework, which provides exposure ages between 8.6 and 3.8% younger. This discrepancy can be explained by a higher spatial variability of the LSD framework than other models, and especially by the model's relative scaling factor high over the Aotearoa New Zealand region during the Holocene (Lifton, 2016). New paleosecular variation records based on Aotearoa New Zealand lake sediment cores (Turner et al., 2015; Turner and Corkill, 2023) suggest that this scaling factor high is a spatial artefact caused by the small number of Southern Hemisphere records used to make up the global model on the LSD framework. Thus, we place greater emphasis on results produced using models that do not contain such effects (e.g., Muscheler et al., 2005; Lifton, 2016).

$^3\text{He}_{\text{cos}}$ production rates have been shown to be indistinguishable in clinopyroxenes and orthopyroxenes (Delunel et al., 2016), justifying our decision to use a worldwide mean production rate estimate for our exposure age determinations. Additionally, this production rate value is supported by a local calibration test using the radiocarbon-dated debris avalanche deposits of the Murimotu Formation, on the outer northwestern slopes of Ruapehu (Eaves et al., 2015). Despite some studies suggesting that olivines concentrate slightly larger amounts of $^3\text{He}_{\text{cos}}$ compared to pyroxenes (Ackert et al., 2003; Fenton et al., 2009), the difference was almost statistically insignificant, and in a more recent study, Fenton and Niedermann (2014, as well as previous data from Blard et al., 2006) provided results implying that olivine and pyroxenes have similar amounts of $^3\text{He}_{\text{cos}}$.

We measured three to five samples per lava flow to counter the possibility that individual samples may be affected by erosion or shielding that would compromise their accuracy for constraining the time of lava flow emplacement. To derive single exposure ages for lava flows from these multiple measurements, we used each sample's internal age uncertainty (1σ , not including the external uncertainty from P_3) and implemented the summary age statistics and outlier removal routine contained in version 3 of the Balco et al. (2008) online exposure age calculator, described in the documentation (section 4.C. available at <https://sites.google.com/a/bgc.org/v3docs/>). In summary, we used weighted mean summary ages if the samples formed a single population at the 95% confidence interval using the chi-squared statistic. If this result could not be achieved by incremental outlier removal while maintaining a sample population ≥ 3 , then we used the mean and standard error as the summary age of the lava flow. We finally propagated the P_3 uncertainty into all summary ages (reported with their 2σ interval), which is necessary when comparing TCN-based eruption ages to those from other geochronological methods (e.g. $^{40}\text{Ar}/^{39}\text{Ar}$). In the case of flows for which less than three samples passed the single population test (or only two samples were analysed), we considered the summary age to be a minimum eruption age. For those flows with three or more exposure ages passing this test, summary ages

were considered robust eruption ages. We used internal 2σ intervals (INT 2σ , not including P_3 errors) to compare intra and
275 inter-site age distributions and clustering.

4 Results

4.1 Bulk rock and mineral geochemistry

Major and trace elements concentrations of bulk rocks and minerals from each of the lava flows studied can be found in Table A2.

280 All bulk rock analyses yielded basaltic andesite to andesitic compositions according to the classification scheme of Le Maitre (2002). Our results indicate that, from the sampled flows, younger flows tend to be less evolved than older flows (Figure 3a).

Most flows have a bulk geochemistry similar to the reported ranges (Conway et al., 2016) for the respective units they were classified as (Townsend et al., 2017). The only exception is the site here referred as NR, which shows higher MgO (6.22 wt.%) and lower Na₂O (2.95 wt.%) than other samples of the Makotuku Member (2-3 wt.% and 3.4–4 wt.%, respectively, Conway
285 et al., 2016). Instead, major element geochemistry of our NR sample matches that of the Mangaehuehu Member (4.7–7 wt.% MgO and 3-3.4 wt.% Na₂O, Conway et al., 2016), the lavas of which are significantly older (Table 1).

Mineral geochemistry shows that, on average, the pyroxenes are pigeonite (Figure 3b), although analyses of modal phases of Ruapehu lavas (Hackett, 1985; Conway, 2016) suggest that this represents a combination of augite and enstatite crystals. MN and Tsa yield average compositions of enstatite phases, indicating that the orthopyroxene phase dominates over the
290 clinopyroxene in these flows. The analysed olivines (sample GR-PD023) are magnesium-rich (Fo₆₉; Table A2). Comparing the obtained average compositions with previous ³He_{cos} studies, our pyroxenes show higher contents of orthopyroxene than those analysed by Blard et al. (2006) and higher clinopyroxene contents than samples of Eaves et al. (2015).

In general, trace element concentrations are relatively homogeneous across the sampled sites. Figure 3c shows the concentrations of the main radioactive elements producing ⁴He_{rad} (U, Th and Sm) in bulk rock and in the mineral phases (pyroxenes and
295 olivines). Bulk rocks contain 0.94–1.74 ppm U, 4.04–6.50 ppm Th and 2.41–3.25 ppm Sm, while pyroxenes contain 0.01–0.10 ppm U, 0.04–0.36 ppm Th, and 0.44–2.07 ppm Sm (uncertainties <20% and detection limits of 0.01 ppm). Note that U and Th concentrations in the rock are not involved in the production of the measured ⁴He_{rad}, as the external crystal rims were removed before the analyses. GR olivines have lower contents of these elements (with U below the detection limit), and therefore larger P_4 associated errors. However, element concentrations provided for minerals represent maximum values, as there is a possibil-
300 ity of groundmass and/or melt inclusion contamination that may be not accounted for at the time of measurement. These values indicate (maximum) partition coefficients (Kd) of 0.006–0.085 for U; 0.006–0.080 for Th and 0.15–0.74 for Sm in pyroxenes and 0.045 for U; 0.045 for Th and 0.11 for Sm in olivines. The pyroxene maximum Kd values, in general, agree with values from the literature (Dostal et al., 1983; Luhr and Carmichael, 1980; Gallahan and Nielsen, 1992; Nicholls and Harris, 1980). Those for U and Th in olivines are similar to those reported by Dunn and Sen (1994) and Villemant (1988), while the Kd for
305 Sm in our olivines is an order of magnitude larger than that of Dunn and Sen (1994), which can be explained by the impact of fluid inclusions with higher Sm contents within the olivine crystals.

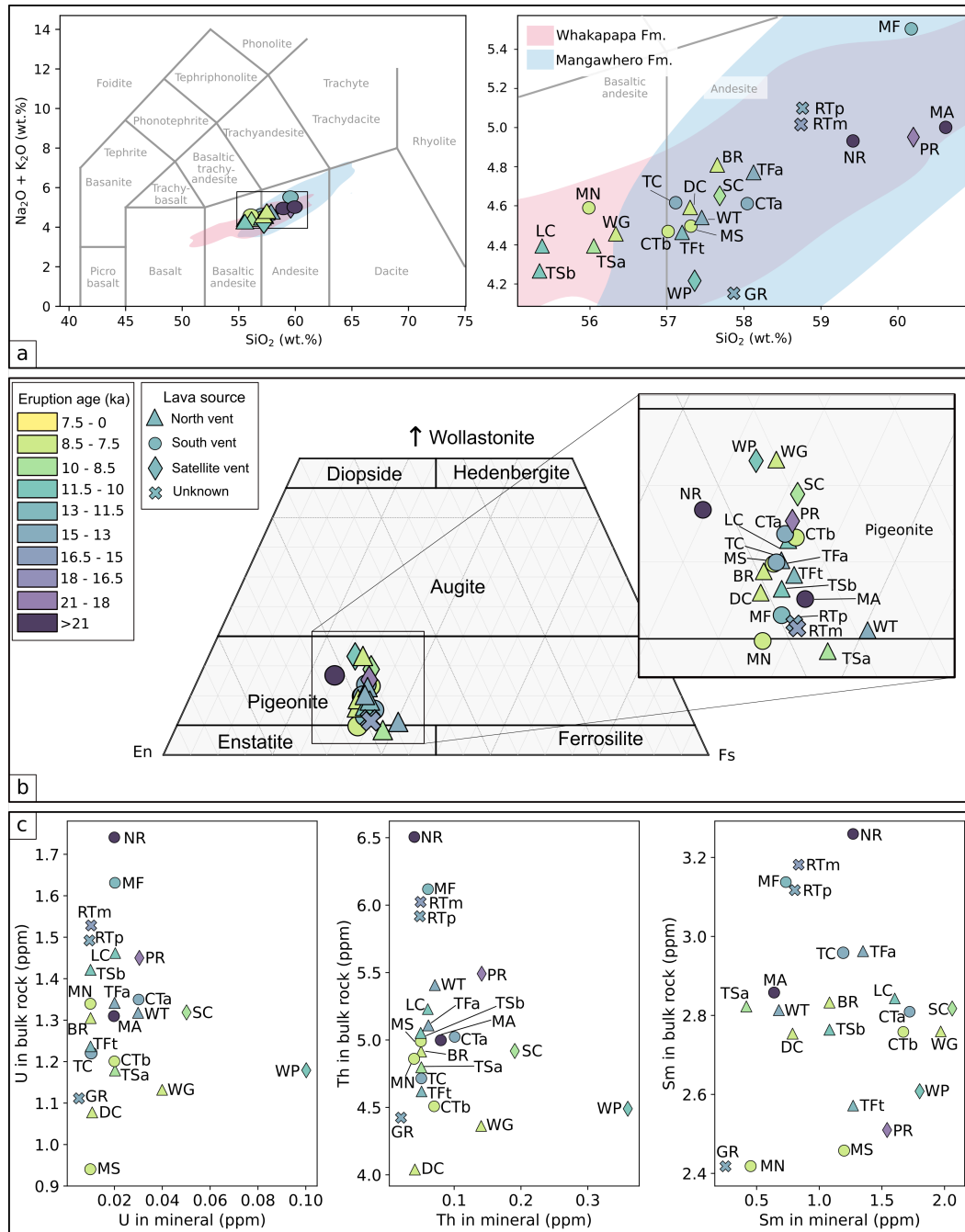


Figure 3. a) TAS classification diagram of the sampled lava flows (Le Maitre, 2002). Coloured areas represent geochemical ranges of Whakapapa and Mangawhero lavas. b) Pyroxene compositions according to the classification scheme of Morimoto et al. (1988). Each triangle represents the average geochemistry of each lava flow's pyroxene population. c) U, Th and Sm concentrations in the samples. x axis represents maximum concentrations in minerals (pyroxenes and olivines) and y axis in bulk rock.

4.2 Local magmatic $^3\text{He}/^4\text{He}$ ratio

We measured ^3He and ^4He released after in-vacuo crushing for samples MA-PD058; WG-PD326; and DC-PD329 (data available in supplementary file S2.1). These values result in $^3\text{He}/^4\text{He}$ ratios of: 5.5 ± 1.0 ; 17.9 ± 6.9 ; and $9.2 \pm 6.1 \times 10^{-6}$ for each sample, respectively. The large uncertainties associated with the ratios measured in samples WG-PD326 and DC-PD329 are a result of the low total ^4He values ($<5 \times 10^9$ at/g).

We used the three measured $^3\text{He}/^4\text{He}$ values and two ratios from Patterson et al. (1994) to constrain the local magmatic $^3\text{He}/^4\text{He}$ value. These are $6.5 \pm 2.4 \times 10^{-6}$ (Ohakune basalt pyroxenes, one sample) and $8.6 \pm 3.7 \times 10^{-6}$ (Waimarino basalt olivines, mean of three aliquots from one sample), which are comparable to those obtained by in-vacuo crushing of our samples. All analyses from Patterson et al. (1994) are from fused samples (and not from in-vacuo crushed samples, which is the standard approach to release predominantly magmatic He, Kurz, 1986b), but we assumed that all the measured ^3He and ^4He has a magmatic origin, as the samples come from flow interiors of young flows (i.e. they likely contain low $^4\text{He}_{\text{rad}}$ and minimal to no $^3\text{He}_{\text{cos}}$). With this data, we calculated an uncertainty-weighted mean $^3\text{He}/^4\text{He}$ ratio using IsoplotR (Vermeesch, 2018) and obtained a value of $5.9 \pm 2.6 \times 10^{-6}$ (or 4.2 ± 1.9 Ra, see supplementary file S2.2), which we used for the magmatic corrections in this study. The impact of the obtained magmatic ratio and its uncertainty in our results is described in subsection 4.3.

4.3 Fusion-released Helium isotopes and cosmogenic ^3He concentrations

We analysed a total of 77 samples from 23 individual flows. All fusion ^3He and ^4He measurements, calculated $^3\text{He}_{\text{cos}}$ concentrations, and derived exposure and eruption ages are shown in Table 2. Measured ^3He varies between 2.1×10^6 and 2.4×10^7 at/g, with 2–7% of relative associated error (1σ). $^4\text{He}_{\text{tot}}$ values are surprisingly low across most of our samples (possibly due to the repeated HF-leaching steps the samples were exposed to prior to analysis, see Bromley et al., 2014), typically ranging between 0.3 and 9.6×10^{10} at/g with uncertainties between 0.04 and 0.18×10^{10} at/g. These values normally result in total $^3\text{He}/^4\text{He}$ ratios of 130–800 Ra, although they are lower (50–90 Ra) or higher (1200–1500 Ra) in some cases (see Table 2).

The complete detail of all sources of corrections is available in Table A3 and in the supplementary file S4. Calculated $^3\text{He}_{\text{nuc}}$ production rates (P_{nuc}) are four orders of magnitude below P_3 values, making $^3\text{He}_{\text{cos}}$ results insensitive to nucleogenic corrections. P_4 ranges between 4×10^4 and 3×10^5 at/g/yr. We assume a 10% error associated with all P_4 results, except for the site GR, which has lower concentrations of radioactive elements (hence, the lowest P_4 number within our lavas) with uncertainties of 20–40%, for which we considered a 25% in our P_4 estimates. Uncertainties associated with the calculated local magmatic $^3\text{He}/^4\text{He}$ ratio represent $<10\%$ of the informed error associated with $^3\text{He}_{\text{cos}}$ results. This ratio, combined with our P_4 calculations (3.5×10^4 – 6.1×10^5 at/g/yr) and local P_3 values between 313 and 584 at/g/yr (elevations between 1288 and 2148 m asl) yields R factors >0.99 (Table A3). This indicates that, even if the measured concentrations of radioactive elements in our minerals represent maximum values, corrections for $^4\text{He}_{\text{rad}}$ have a minor ($<1\%$) impact on our final $^3\text{He}_{\text{cos}}$ values. The $^3\text{He}_{\text{cos}}/^3\text{He}_{\text{tot}}$ ratios calculated for our samples vary between 0.90 and 0.99, implying that the $^3\text{He}_{\text{cos}}$ quota dominates over magmatic (and nucleogenic) ^3He .

The used magmatic $^3\text{He}/^4\text{He}$ ratio ($5.9 \pm 2.6 \times 10^{-6}$; or 4.2 ± 1.9 Ra) is derived from only three samples from Ruapehu
 340 crushed in vacuo (this study) and two samples from the Ohakune and Waimarino basalts (data from fused samples, Patterson
 et al., 1994), and it is therefore not well constrained. However, this does not significantly affect our final results due to the low
 $^4\text{He}_{\text{tot}}$ measured in most of our samples. To demonstrate this, we estimated the resulting $^3\text{He}_{\text{cos}}$ concentration if the magmatic
 $^3\text{He}/^4\text{He}$ ratio of the sample SC-PD001 (which has the smallest measured $^3\text{He}/^4\text{He}$ ratio across our samples, and is hence
 the most sensitive to this test) was 8.4 Ra and 2.1 Ra (twice and half the mean value of 4.2 Ra used for our calculations,
 345 and covering most of the range globally observed in subduction zone volcanism, Hilton et al., 2002). This test yields $^3\text{He}_{\text{cos}}$
 concentrations of 3.28 ± 0.31 and $3.71 \pm 0.31 \times 10^6$ at/g (resulting in exposure ages of 9.74 ± 0.85 and 10.91 ± 0.83 ka) with
 magmatic ratios of 8.4 and 2.1 Ra, respectively, both falling within the error of the concentration obtained using a magmatic
 ratio of 4.2 ± 1.9 Ra for SC-PD001 ($3.57 \pm 0.31 \times 10^6$ at/g; exposure age 10.53 ± 0.83 ka). This indicates that the potentially
 variable magmatic $^3\text{He}/^4\text{He}$ ratios present in our samples do not significantly impact our results, although they might partially
 350 explain small differences between the obtained exposure ages of samples from the same flow.

4.4 Lava flows: background and new ^3He constraints

We obtained 16 eruption ages and seven minimum eruption ages (Table 2) based on the criteria defined in subsection 3.6.2.

4.4.1 Iwikau Member

The Iwikau Member of the Whakapapa Formation covers a large area on the northwestern and eastern flanks of Ruapehu
 355 (Figure 1), and is subdivided into three flow packages: Tawhainui, Mangatoetoenui, and Taranaki Falls flows (Figure 4a, b), all
 interpreted to have originated from Ruapehu's northern vent (Townsend et al., 2017).

Tawhainui flows

The Tawhainui flows comprise a voluminous sequence of lava flows on the northwestern slopes of the volcano. They have
 been the most studied unit of Ruapehu due to their accessibility and availability of the fresh exposures of flow interiors,
 360 facilitated by the construction of the largest ski field in Te Ika-a-Māui North Island. We sampled three flows from this unit:
 Delta Corner flow (DC samples), Bruce Road flow (BR samples, both after Greve et al., 2016), and Whakapapa Glacier flow
 (WG samples).

The fresh-looking Delta Corner flow has been previously dated at 6.0 ± 2.4 ka with $^{40}\text{Ar}/^{39}\text{Ar}$ by Conway et al. (2016), age
 refined to 8200–7900 BP by Greve et al. (2016) based on paleomagnetic data. Analyses from three samples from an area with
 365 distinct 'a'ā surface morphologies (see Figure 2b) yield well clustered exposure ages, which result in an eruption age of $7.8 \pm$
 1.5 ka. Our result shows perfect agreement with the age range of 8200–7900 BP provided by Greve et al. (2016), suggesting
 that the flow's true age lies on the upper end of the uncertainty provided by Conway et al. (2016).

The Bruce Road flow is a large 'a'ā flow that underlies the Delta Corner flow, and that has been constrained to 8800–8500
 BP by Greve et al. (2016) using paleomagnetism. Downslope from the BR sample site, the flow has unclear boundaries, as it is

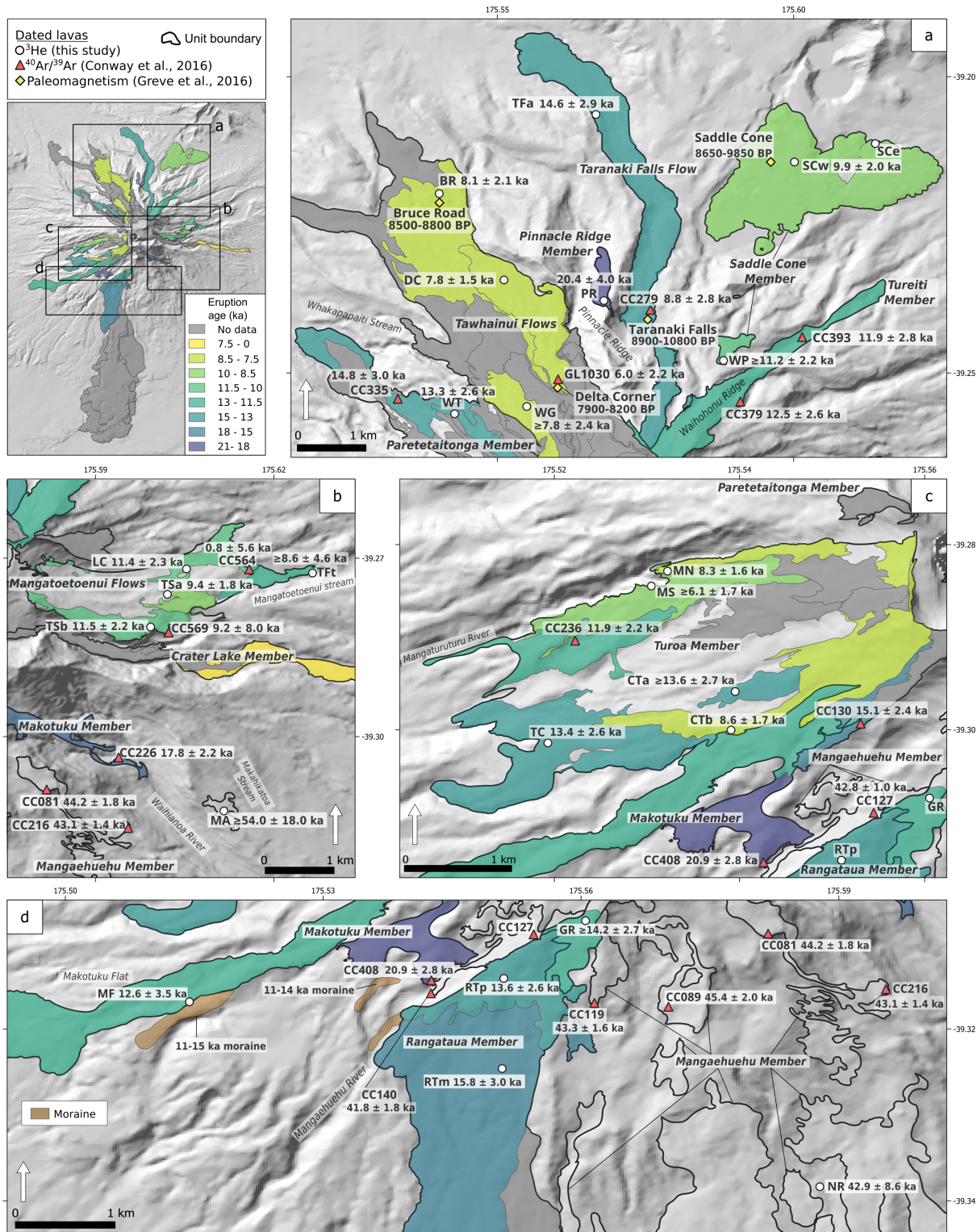


Figure 4. Map of dated <21 ka lava flows on: a) northern, b) eastern, c) western, d) southern Ruapehu. Polygons redefined from Townsend et al. (2017). Boundaries of the Mangaehuehu Member (Mangawhero Formation) as of Townsend et al. (2017) shown for context of site NR of this study. Grey polygons represent postglacial flows without chronological data.

370 covered by vegetation. Based on four individual exposure ages (7.4, 8.1, 7.8 and 9.1 ka), we obtained an eruption age of 8.1 ± 2.1 ka for the Bruce Road flow, which is consistent with its paleomagnetic constraint.

The Whakapapa Glacier flow is one of the youngest lavas of the sequence based on stratigraphic relations, which suggest a comparable age to that of the Delta Corner flow. Due to the highly eroded nature of the Whakapapa Glacier flow's surface, only two WG samples were collected, which yield a minimum eruption age of 7.8 ± 2.4 ka. This result is consistent with the
375 stratigraphy and the age of the Delta Corner flow.

Mangatoetoenui flows

This subunit includes a group of lava flows on the eastern slopes of Ruapehu and its age is poorly constrained (Table 1). We sampled four individual flows classified based on geochemistry and location within the Mangatoetoenui flows: Lava Cascade (LC samples), Tukino Slopes-a (TSa samples), Tukino Slopes-b (TSb samples), and Tukino Flats (TFt samples) flows
380 (Figure 4b).

The LC sample site is interpreted to be part of an approximately 4-km long lava flow terminating at a 20 m high lava cascade at 1620 m asl. This flow was described in detail by Rhodes (2012) and dated on a cliff at its terminus at 0.8 ± 5.6 ka by Conway et al. (2016). We analysed four individual samples from an outcrop located ~1 km upslope from the lava toe and obtained an eruption age of 11.4 ± 2.3 ka for the Lava Cascade flow (outside the 2σ interval of Conway et al., 2016, see subsection 5.1),
385 with one young outlier removed (sample LC-PD256). The outlier can be explained by local erosion, shielding from a now collapsed neighbouring lava tumuli (and hence an underestimation of the shielding factor) or a period of tephra cover that could have reduced the ^3He production on the surface sampled.

The Tukino Slopes-a flow has not been previously dated, but its location and stratigraphic position suggest a similar eruption age to the Lava Cascade and Tukino Slopes-b flows. All measured TSa samples (8.7, 9.5 and 9.9 ka) form a single population
390 and provide an eruption age of 9.4 ± 1.8 ka, in good agreement with the stratigraphy.

The TSb sample site likely corresponds to the same flow dated with $^{40}\text{Ar}/^{39}\text{Ar}$ at 9.2 ± 8.0 by Conway et al. (2016). We obtained exposure ages of 10.5, 11.9, and 11.9 ka for the TSb samples, which result in a refined eruption age of 11.5 ± 2.2 ka for the Tukino Slopes-b flow. The eruption age we obtained for the Tukino Slopes-b flow is consistent with (and more precise than) the existing radiometric age and, as suggested by the stratigraphy, similar to the age of the Tukino Slopes-a flow.

395 The TFt sample site is located at a lower elevation (~1515 m asl), and its stratigraphic position suggest a similar or older age than the rest of the Mangatoetoenui flows. Our results for three TFt samples (7.7, 10.8 and 7.3 ka) do not form a single population, and result in a minimum eruption age of 8.6 ± 4.6 ka for the Tukino Flats flow. The older exposure age (10.8 ka) is difficult to explain as an outlier, as the presence of inherited ^3He is not justifiable for lava flows, whereas the younger ages may be explained as outliers owing to surface erosion or temporal burial by alluvium or tephra. Lack of additional samples
400 hindered our ability to obtain a robust eruption age. Considering a minimum eruption age of 8.6 ± 4.6 ka, the ages of the other flows from the Mangatoetoenui flows, and their stratigraphic position, our best estimate for the Tukino Flats flow is 12–10 ka.

Taranaki Falls flow

The Taranaki Falls flow (TFa samples) is a rootless (not continuous towards the vent it would have been erupted from) elongated lava flow which outcrops discontinuously for ~8 km almost directly to the north of the volcano's summit area

405 (Townsend et al., 2017, Figure 4a) and terminates at the 20 m waterfall after which it is named. The flow was dated with $^{40}\text{Ar}/^{39}\text{Ar}$ at 8.8 ± 2.8 ka by Conway et al. (2016). Based on this date, Greve et al. (2016) found two age ranges (10 800–10 200 and 9500–8900 BP) with better match to the local paleosecular variation record.

We sampled the flow at an outcrop 800 m upstream from the flow terminus and obtained exposure ages of 14.6, 14.2, and 15.0 ka, resulting in an eruption age of 14.6 ± 2.9 ka, outside the confidence interval of the radiometric age (see subsection 5.1).

410 4.4.2 Saddle Cone Member

This unit comprises a large, lobate 'a'ā flow originating from a parasitic cone on the north-northeastern side of Ruapehu, almost disconnected from the main edifice (Figure 4a). The only available constraint for this flow was provided by Greve et al. (2016), who suggested an age of 9850–8650 BP based on paleomagnetic analyses of samples from the western lobe of the flow. The Saddle Cone Member also includes a smaller blocky lava flow lying between this cone and Ruapehu's summit region (that
415 likely originated from a satellite vent), adjacent to the Waihohonu Ridge and here referred to as the Waihohonu Plateau flow, linked to the main Saddle Cone deposits by its geochemical similarity and location. Nairn et al. (1998) suggested that the Waihohonu Plateau ("1990 m lava" therein) might be younger than 5 ka, as no deposits from the Papakai Tephra were found above the flow.

Individual exposure ages of samples from the main western lobe of the Saddle Cone lavas (SCw samples; 10.5, 10.2 and 9.2
420 ka) show good agreement. We additionally analysed a sample from the eastern lobe (SCe, whose surface elevation is more than 100 m below that of the main lobe, see Figure 4a) to test the hypothesis of a multi-episodic origin. The obtained exposure age of this sample is 9.6 ka (Table 2), indistinguishable from those of the western lobe. We suggest a single eruption age for both lobes of 9.9 ± 2.0 ka ($n=4$), consistent with the existing paleomagnetic constraint for this flow.

The blocky nature of the Waihohonu Plateau flow made it difficult to find uneroded surfaces, and only two samples were
425 obtained (WP samples). Analyses from these samples result in a minimum eruption age of 11.2 ± 2.2 ka.

4.4.3 Pinnacle Ridge Member

The Pinnacle Ridge Member is a welded spatter deposit linked to a dike on a ridge of the same name on the northern flanks of the volcano (Figure 4a). Due to its geochemistry and geographic location, Donoghue et al. (1999) linked this isolated spatter-fed lava deposit to the Taurewa pyroclastic unit (*ca* 10 ka) described by Topping and Kohn (1973), manifested as a tephra layer
430 with isopachs centered on the northern flanks of Ruapehu.

PR samples yield exposure ages of 20.8, 19.0 and 21.5 ka, resulting in an eruption age of 20.4 ± 4.0 ka for this unit, at least 10 kyr prior to the Taurewa eruptive event.

4.4.4 Rangataua Member

The Rangataua Member includes the longest and most voluminous known lava flow of Ruapehu (≥ 15 km long; ~ 1.5 km³). It
435 first outcrops ~ 3.5 km south from the summit, which led to the hypothesis that it is sourced from a satellite vent (Hackett, 1985;

Price et al., 2012), although Townsend et al. (2017) suggest initial transport over ice as a possible alternative explanation for its rootless nature. Based on geochemical differences, this unit was first subdivided by Price et al. (2012) into proximal, medial and distal flows (the latter being the largest flow of the sequence), who suggested eruption ages of 12–10 ka based on under- and overlying tephra sequences (unpublished data). These lavas overlie at 1600–1400 m asl left lateral moraines which have
440 been correlated to right lateral moraines of the Mangaehuehu River valley dated at 11–14 ka (Eaves et al., 2019) using $^3\text{He}_{\text{cos}}$ dating (Figure 4d). We sampled the Rangataua Member at two locations; one close to the highest outcrops (RTp, "proximal"), and another one approximately 1 km to the south (RTm, "medial"). We did not sample the distal flows, which are interpreted to be older than the medial flows, due to vegetation cover (Figure 1c).

RTp samples yield exposure ages of 13.9, 12.4, 13.9 and 14.4 ka and a final eruption age of 13.6 ± 2.6 ka. Results of RTm
445 samples (16.2, 16.0, 15.3 and 8.2 ka) include a young outlier, but the remaining samples are internally consistent and indicate an eruption age of 15.8 ± 3.0 ka, which agrees with the field relationships of the area, as this flow underlies RTp, but not so with previous age estimates (see subsection 5.1). The ages of the Rangataua proximal and medial flows and their INT 2σ uncertainties (13.6 ± 0.6 and 15.8 ± 0.8 , respectively) do not overlap, indicating that they correspond to different eruptive episodes.

450 4.4.5 Paretetaitonga Member

The Paretetaitonga Member comprises a series of lava flows that likely originated from the northern summit vent of Ruapehu and emplaced in the headwaters of the Whakapapaiti Stream, northwest of the summit area (Figure 4a). We sampled one lava (Whakapapaiti flow, WT samples) stratigraphically higher than the only flow dated from this unit (14.8 ± 3.0 ka, Conway et al., 2016).

455 We obtained exposure ages in good agreement with each other (12.8, 13.4 and 13.7 ka), resulting in an eruption age of 13.3 ± 2.6 ka, consistent with the existing chronology.

4.4.6 Turoa Member

The Turoa Member corresponds to a sequence of numerous flows extending directly west from the edge of Ruapehu's crater rim and reaching the Mangaturuturu valley bottom. Based on the distributions of the flows and two $^{40}\text{Ar}/^{39}\text{Ar}$ dates (Table 1),
460 this unit is assumed to have been formed by effusive activity from the southern summit vent at *ca* 170–10 ka. We sampled five sites, distributed on the northern (MN, MS), central (CTa, CTb) and western (TC) areas (Figure 4c) covered by this unit.

The Mangaturuturu North flow corresponds to a flow on the headwaters of the Mangaturuturu Stream, and due to stratigraphic relations and flow morphologies, was suspected to be the youngest lava on western Ruapehu. We analysed five surfaces of the Mangaturuturu North flow (MN samples, with exposure ages of 8.0, 8.9, 6.0, 8.9 and 7.7 ka), and eliminating the young
465 outlier of 6.0 ka, they yield a robust eruption age of 8.3 ± 1.6 ka.

The Mangaturuturu South flow underlies the Mangaturuturu North flow, and extends down ~3 km from the summit area. Poor exposures of original flow surfaces prevented us from collecting more than three samples from the Mangaturuturu South flow (MS samples). Additionally, purification of the minerals in these samples was incomplete due to high (>50%) mass loss

with each HF leaching cycle, and we suspect an overestimation of measured pyroxene mass for these samples. Sample analyses
470 result in exposure ages that do not pass the single population test (Table 2), but provide a minimum eruption age of 6.1 ± 1.7
ka.

Central Turoa-a/b flows are located close to each other and at a similar elevation, south of the MN and MS sample sites. We
only collected two samples from the Central Turoa-a flow (CTa) due to a lack of suitable surfaces, which suggest a minimum
eruption age of 13.6 ± 2.7 ka. Three out of four Central Turoa-b flow samples analysed (Ctb samples, with exposure ages of
475 4.9, 8.8, 8.4 and 8.5) show good agreement and yield an eruption age of 8.6 ± 1.7 ka. These results indicate that the Central
Turoa-a and -b flows correspond to two different eruptive episodes.

The Turoa Cascades flow (TC samples) is a large flow that reaches the Mangaturuturu River valley floor, and its stratigraphic
position indicates that it is likely the oldest flow of the Turoa Member. Individual exposure ages of the TC samples (11.4, 14.1,
13.1 and 13.3 ka) include a young outlier and indicate an eruption age of 13.4 ± 2.6 ka for the Turoa Cascades flow, in good
480 agreement with the rest of the ages obtained for the Turoa Member lavas.

4.4.7 Makotuku Member (Mangawhero Formation)

We sampled three flows previously mapped as part of the Makotuku Member of the Mangawhero Formation; Makotuku Flat
flow (MF samples) on the southwest, and Ngā Rimutāmaka and Makahikatoa flows (NR and MA samples, named after local
site and stream, respectively) on the south of Ruapehu's edifice. The spatial distribution of Makotuku lavas suggest that they
485 originated from the southern summit vent.

The Makotuku Flats flow extends to the west of the edifice reaching the Makotuku valley bottom (Figure 4d), and overlies a
11–15 ka moraine (Townsend et al., 2017) at the sampled site. Although results of analyses of MF samples are not particularly
well clustered, they behave as a single population and provide an eruption age of 12.6 ± 3.5 ka.

Analyses of NR samples yield well clustered exposure ages, and we interpret an eruption age of 42.9 ± 8.6 ka, which
490 corresponds to the only date provided for this lava flow so far. It is worth noting that this age and the geochemical composition
of this flow match with the $^{40}\text{Ar}/^{39}\text{Ar}$ ages and high-MgO/low- Al_2O_3 nature of Mangaehuehu Member lavas (Table 1).

The small area where the Makahikatoa flow outcrops prevented us from obtaining more than two suitable samples, which
result in a minimum eruption age of 54.0 ± 18.0 ka, the first age constraint for this flow.

These three eruption ages do not contradict previous chronology nor the stratigraphy, but they do not match the age ranges
495 indicated by the geochemical affinities for the Makotuku Member lavas as described by Conway et al. (2016) and Townsend
et al. (2017, see subsection 5.2).

4.4.8 Mangaehuehu Member (Mangawhero Formation)

We sampled a lava flow (Girdlestone Ridge, GR samples) outcropping on a ridge top ~1.5 km south from Ruapehu's summit
and 800 m southwest from Girdlestone peak. This site was previously mapped as Mangaehuehu Member lavas (Townsend
500 et al., 2017) based on interpretation of aerial imagery. However, the uneroded aspect of the flow's surface observed in the field

during this study suggests that it could be younger than previously interpreted. The mineral separation process applied to all samples produced the only olivine concentrate (with a minor pyroxene population) of this study.

Analyses of these samples indicate a minimum eruption age of 14.2 ± 2.7 ka (mean calculated from the two oldest exposure ages after the elimination of two outliers), which represents the first age constraint for this lava flow.

Table 2: Results of Helium isotopes measurements and exposure ages by sample.

Sample	Latitude (S)	Longitude (E)	Elevation (MSL)	Shielding factor	$^3\text{He}_{\text{tot}} \pm 1\sigma$ (10^6 at/g)	$^4\text{He}_{\text{tot}} \pm 1\sigma$ (10^{10} at/g)	Total $^3\text{He}/^4\text{He}$ (R/Ra)	$^3\text{He}_{\text{cos}} \pm 1\sigma$ (10^6 at/g)	Exposure age $\pm 1\sigma$ (ka)
DC - Delta Corner flow			Tawhainui flows - Iwikau Member						
DC-PD327	39.2346	175.5515	1600.4	0.999	2.82 ± 0.21	0.72 ± 0.05	283 ± 28	2.78 ± 0.21	7.52 ± 0.50
DC-PD329	39.2342	175.5509	1591.8	0.999	3.08 ± 0.23	0.98 ± 0.05	227 ± 20	3.03 ± 0.23	8.22 ± 0.56
DC-PD330	39.2341	175.5507	1590.3	0.999	2.89 ± 0.22	0.80 ± 0.05	260 ± 26	2.85 ± 0.22	7.72 ± 0.52
Eruption age of DC: 7.8 ± 1.5 ka INT 2σ : 0.6 ka									
BR - Bruce Road flow			Tawhainui flows - Iwikau Member						
BR-PD014	39.2201	175.5405	1360.0	0.999	2.33 ± 0.12	0.61 ± 0.05	277 ± 26	2.30 ± 0.13	7.37 ± 0.35
BR-PD016	39.2198	175.5379	1359.2	0.982	2.57 ± 0.14	1.45 ± 0.06	128 ± 9	2.49 ± 0.14	8.05 ± 0.41
BR-PD017	39.2190	175.5409	1332.6	0.998	2.47 ± 0.14	1.65 ± 0.08	108 ± 8	2.38 ± 0.15	7.75 ± 0.43
BR-PD018	39.2190	175.5411	1332.4	0.998	2.87 ± 0.16	1.14 ± 0.08	181 ± 16	2.81 ± 0.16	9.13 ± 0.50
Eruption age of BR: 8.1 ± 2.1 ka INT 2σ : 1.5 ka									
WG - Whakapapa Glacier flow			Tawhainui flows - Iwikau Member						
WG-PD325	39.2557	175.5551	2079.1	0.991	4.44 ± 0.22	0.91 ± 0.05	351 ± 26	4.40 ± 0.22	8.51 ± 0.39
WG-PD326	39.2556	175.5549	2066.7	0.995	3.67 ± 0.19	1.15 ± 0.07	230 ± 18	3.61 ± 0.19	7.13 ± 0.33
Minimum eruption age of WG: 7.8 ± 2.4 ka INT 2σ : 2.0 ka									
LC - Lava Cascade flow			Mangatoetoenui flows - Iwikau Member						
LC-PD254	39.2718	175.6052	1827.1	0.997	5.13 ± 0.36	1.22 ± 0.05	303 ± 25	5.07 ± 0.37	11.38 ± 0.75
LC-PD255	39.2718	175.6053	1826.6	0.997	5.01 ± 0.36	1.75 ± 0.06	206 ± 16	4.91 ± 0.36	11.14 ± 0.74
LC-PD256	39.2718	175.6053	1825.6	0.996	3.99 ± 0.29	1.46 ± 0.05	197 ± 16	3.91 ± 0.29	9.02 ± 0.62 *
LC-PD257	39.2718	175.6053	1824.7	0.996	5.28 ± 0.33	0.89 ± 0.05	430 ± 37	5.24 ± 0.33	11.64 ± 0.68
Eruption age of LC: 11.4 ± 2.3 ka INT 2σ : 0.8 ka									
TSa - Tukino Slopes-a flow			Mangatoetoenui flows - Iwikau Member						
TSa-PD205	39.2761	175.6021	1905.1	0.983	3.98 ± 0.22	0.51 ± 0.10	570 ± 120	3.96 ± 0.23	8.74 ± 0.46
TSa-PD206	39.2761	175.6021	1905.9	0.997	4.41 ± 0.24	0.14 ± 0.08	2300 ± 1300	4.41 ± 0.24	9.51 ± 0.47
TSa-PD207	39.2761	175.6021	1905.5	0.997	4.61 ± 0.23	0.55 ± 0.06	600 ± 68	4.58 ± 0.23	9.85 ± 0.46
Eruption age of TSa: 9.4 ± 1.8 ka INT 2σ : 0.5 ka									
TSb - Tukino Slopes-b flow			Mangatoetoenui flows - Iwikau Member						
TSb-PD209	39.2815	175.5993	1932.5	0.997	5.06 ± 0.15	^4He below detection limit		5.06 ± 0.31	10.47 ± 0.59
TSb-PD210	39.2815	175.5992	1935.0	0.989	5.86 ± 0.28	1.41 ± 0.10	299 ± 25	5.78 ± 0.28	11.92 ± 0.54
TSb-PD211	39.2816	175.5993	1929.2	0.993	5.78 ± 0.28	0.80 ± 0.05	522 ± 44	5.74 ± 0.28	11.90 ± 0.55
Eruption age of TSb: 11.5 ± 2.2 ka INT 2σ : 0.6 ka									

Table 2: Continued.

Sample	Latitude (S)	Longitude (E)	Elevation (MSL)	Shielding factor	$^3\text{He}_{\text{tot}} \pm 1\sigma$ (10^6 at/g)	$^4\text{He}_{\text{tot}} \pm 1\sigma$ (10^{10} at/g)	Total $^3\text{He}/^4\text{He}$ (R/Ra)	$^3\text{He}_{\text{cos}} \pm 1\sigma$ (10^6 at/g)	Exposure age $\pm 1\sigma$ (ka)
TFt - Tukino Flats flow			<i>Mangatoetoenui flows - Iwikau Member</i>						
TFt-PD212	39.2726	175.6261	1521.2	0.994	2.71 ± 0.20	0.95 ± 0.06	206 ± 20	2.66 ± 0.21	7.71 ± 0.53
TFt-PD213	39.2726	175.6263	1522.0	0.998	3.86 ± 0.27	1.03 ± 0.04	270 ± 22	3.80 ± 0.28	10.77 ± 0.71
TFt-PD214	39.2723	175.6271	1506.4	0.988	2.47 ± 0.14	0.68 ± 0.06	263 ± 27	2.43 ± 0.14	7.28 ± 0.36
<i>Minimum eruption age of TFt: 8.6 ± 4.6 ka INT 2σ: 4.3 ka</i>									
TFa - Taranaki Falls flow			<i>Taranaki Falls flow - Iwikau Member</i>						
TFa-PD088	39.2067	175.5668	1308.2	0.999	4.65 ± 0.29	1.64 ± 0.06	204 ± 15	4.56 ± 0.29	14.62 ± 0.85
TFa-PD090	39.2060	175.5665	1302.8	0.996	4.38 ± 0.27	1.01 ± 0.05	312 ± 24	4.33 ± 0.27	14.23 ± 0.82
TFa-PD091	39.2059	175.5664	1288.2	0.999	4.69 ± 0.29	1.14 ± 0.04	296 ± 21	4.63 ± 0.29	15.04 ± 0.85
<i>Eruption age of TFa: 14.6 ± 2.9 ka INT 2σ: 1.0 ka</i>									
SCw - Saddle Cone flow (western lobe)			<i>Saddle Cone Member</i>						
SC-PD001	39.2143	175.6011	1439.0	0.998	3.85 ± 0.28	5.14 ± 0.12	54 ± 4	3.57 ± 0.31	10.53 ± 0.83
SC-PD002	39.2143	175.6010	1439.3	0.998	3.59 ± 0.26	3.03 ± 0.08	85 ± 7	3.43 ± 0.27	10.15 ± 0.75
SC-PD003	39.2146	175.5997	1443.3	0.998	3.45 ± 0.25	3.91 ± 0.09	63 ± 5	3.24 ± 0.27	9.54 ± 0.73
SCe - Saddle Cone flow (eastern lobe)									
SC-PD093	39.2115	175.6139	1308.18	0.993	2.97 ± 0.22	0.92 ± 0.05	233 ± 21	2.94 ± 0.22	9.64 ± 0.67
<i>Eruption age of SC: 9.9 ± 2.0 ka INT 2σ: 0.7 ka</i>									
WP - Waihothonu Plateau flow			<i>Saddle Cone Member</i>						
WP-PD007	39.2479	175.5882	1911.7	0.996	5.63 ± 0.23	2.06 ± 0.07	197 ± 11	5.55 ± 0.24	11.60 ± 0.45
WP-PD008	39.2479	175.5882	1912.1	0.995	5.22 ± 0.22	1.94 ± 0.03	194 ± 9	5.14 ± 0.23	10.81 ± 0.43
<i>Minimum eruption age of WP: 11.2 ± 2.2 ka INT 2σ: 0.6 ka</i>									
PR - Pinnacle Ridge spatter deposit			<i>Pinnacle Ridge Member</i>						
PR-PD083	39.2370	175.5672	1730.7	0.979	9.39 ± 0.44	6.56 ± 0.20	103 ± 6	9.03 ± 0.48	20.82 ± 1.00
PR-PD084	39.2386	175.5689	1860.9	0.988	9.42 ± 0.44	7.72 ± 0.24	88 ± 5	8.99 ± 0.49	19.04 ± 0.93
PR-PD085	39.2385	175.5688	1857.9	0.997	10.69 ± 0.49	5.84 ± 0.18	132 ± 7	10.37 ± 0.52	21.48 ± 1.00
<i>Eruption age of PR: 20.4 ± 4.0 ka INT 2σ: 1.1 ka</i>									
RTp - Rangataua proximal flow			<i>Rangataua Member</i>						
RTp-PD027	39.3140	175.5509	1831.4	0.997	6.38 ± 0.25	1.74 ± 0.08	264 ± 16	6.28 ± 0.26	13.88 ± 0.53
RTp-PD028	39.3140	175.5509	1833.1	0.996	5.73 ± 0.26	2.13 ± 0.12	194 ± 14	5.61 ± 0.26	12.41 ± 0.56
RTp-PD029	39.3140	175.5509	1832.9	0.996	6.42 ± 0.36	2.24 ± 0.18	206 ± 20	6.29 ± 0.37	13.88 ± 0.75
RTp-PD030	39.3143	175.5512	1816.4	0.988	6.45 ± 0.31	0.98 ± 0.06	474 ± 35	6.40 ± 0.31	14.35 ± 0.62
<i>Eruption age of RTp: 13.6 ± 2.6 ka INT 2σ: 0.6 ka</i>									
RTm - Rangataua medial flow			<i>Rangataua Member</i>						
RTm-PD045	39.3234	175.5520	1585.9	0.991	6.30 ± 0.38	1.83 ± 0.07	248 ± 17	6.20 ± 0.38	16.22 ± 0.91
RTm-PD046 (a)	39.3249	175.5508	1567.6	0.979	6.14 ± 0.25	0.74 ± 0.05	601 ± 48	6.10 ± 0.25	
RTm-PD046 (b)	39.3249	175.5508	1567.6	0.979	5.98 ± 0.30	0.98 ± 0.08	438 ± 43	5.93 ± 0.30	
RTm-PD046 mean	39.3249	175.5508	1567.6	0.979				6.04 ± 0.27	16.03 ± 0.64
RTm-PD047	39.3251	175.5503	1567.4	0.997	5.91 ± 0.29	1.13 ± 0.06	376 ± 28	5.85 ± 0.29	15.27 ± 0.68
RTm-PD048	39.3250	175.5503	1567.3	0.997	3.08 ± 0.16	1.64 ± 0.07	135 ± 9	2.99 ± 0.16	$8.17 \pm 0.40^*$
<i>Eruption age of RTm: 15.8 ± 3.0 ka INT 2σ: 0.8 ka</i>									

Table 2: Continued.

Sample	Latitude (S)	Longitude (E)	Elevation (MSL)	Shielding factor	$^3\text{He}_{\text{tot}} \pm 1\sigma$ (10^6 at/g)	$^4\text{He}_{\text{tot}} \pm 1\sigma$ (10^{10} at/g)	Total $^3\text{He}/^4\text{He}$ (R/Ra)	$^3\text{He}_{\text{cos}} \pm 1\sigma$ (10^6 at/g)	Exposure age $\pm 1\sigma$ (ka)
WT - Whakapapaitei flow			Paretaitonga Member						
WT-PD073	39.2569	175.5428	1892.4	0.987	6.01 ± 0.28	0.35 ± 0.08	1230 ± 270	6.00 ± 0.28	12.78 ± 0.59
WT-PD074	39.2569	175.5428	1892.5	0.991	6.36 ± 0.26	0.73 ± 0.04	624 ± 39	6.33 ± 0.27	13.41 ± 0.54
WT-PD075	39.2560	175.5397	1785.0	0.990	6.06 ± 0.26	1.24 ± 0.05	352 ± 20	6.00 ± 0.27	13.74 ± 0.57
Eruption age of WT: 13.3 ± 2.6 ka INT 2σ : 0.7 ka									
MN - Mangaturuturu North flow			Turoa Member						
MN-PD217	39.2829	175.5322	1815.9	0.993	3.49 ± 0.24	0.30 ± 0.05	830 ± 150	3.48 ± 0.24	7.99 ± 0.50
MN-PD218	39.2829	175.5321	1813.9	0.993	3.82 ± 0.23	0.37 ± 0.04	739 ± 97	3.80 ± 0.23	8.85 ± 0.51
MN-PD219	39.2829	175.5321	1812.1	0.993	2.47 ± 0.19	0.42 ± 0.05	770 ± 200	2.46 ± 0.19	5.99 ± 0.39 *
MN-PD220	39.2829	175.5322	1817.5	0.993	3.91 ± 0.25	0.77 ± 0.03	668 ± 89	3.89 ± 0.25	8.89 ± 0.54
MN-PD221	39.2829	175.5325	1822.8	0.993	3.30 ± 0.20	0.08 ± 0.04	1340 ± 400	3.29 ± 0.20	7.66 ± 0.42
Eruption age of MN: 8.3 ± 1.6 ka INT 2σ : 0.5 ka									
MS - Mangaturuturu South flow			Turoa Member						
MS-PD222	39.2845	175.5304	1750.6	0.954	2.58 ± 0.16	0.50 ± 0.04	371 ± 35	2.55 ± 0.16	6.67 ± 0.35
MS-PD223	39.2845	175.5305	1751.4	0.992	2.51 ± 0.17	0.12 ± 0.05	1560 ± 710	2.51 ± 0.17	6.32 ± 0.36
MS-PD224	39.2845	175.5305	1750.9	0.992	2.08 ± 0.16	0.40 ± 0.11	370 ± 100	2.06 ± 0.16	5.33 ± 0.37
Minimum eruption age of MS: 6.1 ± 1.7 ka INT 2σ : 1.4 ka									
CTa - Central Turoa-a flow			Turoa Member						
CTa-PD229	39.2958	175.5395	1924.0	0.996	6.57 ± 0.33	2.35 ± 0.09	201 ± 13	6.45 ± 0.34	13.24 ± 0.67
CTa-PD230	39.2959	175.5396	1925.1	0.996	6.93 ± 0.36	2.76 ± 0.11	181 ± 12	6.78 ± 0.37	13.89 ± 0.69
Minimum eruption age of CTa: 13.6 ± 2.7 ka INT 2σ : 1.0 ka									
CTb - Central Turoa-b flow			Turoa Member						
CTb-PD231	39.2998	175.5392	1877.5	0.996	2.11 ± 0.14	0.66 ± 0.06	230 ± 25	2.07 ± 0.14	4.93 ± 0.30 *
CTb-PD232	39.3001	175.5390	1873.2	0.991	4.00 ± 0.24	0.74 ± 0.05	390 ± 33	3.96 ± 0.24	8.79 ± 0.49
CTb-PD233	39.3001	175.5390	1872.0	0.994	3.86 ± 0.25	0.93 ± 0.06	298 ± 28	3.81 ± 0.25	8.39 ± 0.52
CTb-PD234 (a)	39.3003	175.5391	1873.4	0.996	3.80 ± 0.24	0.90 ± 0.07	283 ± 28	3.75 ± 0.24	
CTb-PD234 (b)	39.3003	175.5391	1873.4	0.996	3.96 ± 0.27	0.60 ± 0.05	472 ± 50	3.93 ± 0.26	
CTb-PD234 mean	39.3003	175.5391	1873.4	0.996				3.85 ± 0.25	8.47 ± 0.51
Eruption age of CTb: 8.6 ± 1.7 ka INT 2σ : 0.6 ka									
TC - Turoa Cascades flow			Turoa Member						
TC-PD066	39.3014	175.5193	1533.2	0.997	4.13 ± 0.20	1.03 ± 0.06	288 ± 23	4.07 ± 0.21	11.37 ± 0.53 *
TC-PD067	39.3015	175.5192	1533.6	0.997	5.24 ± 0.27	1.14 ± 0.05	331 ± 21	5.18 ± 0.26	14.09 ± 0.65
TC-PD068	39.3015	175.5192	1533.1	0.997	4.74 ± 0.23	1.09 ± 0.04	313 ± 18	4.68 ± 0.23	13.05 ± 0.62
TC-PD070	39.3012	175.5193	1528.0	0.997	4.89 ± 0.23	0.82 ± 0.04	431 ± 28	4.85 ± 0.23	13.27 ± 0.61
Eruption age of TC: 13.4 ± 2.6 ka INT 2σ : 0.7 ka									
MF - Makotuku Flats flow			Makotuku Member						
MF-PD061	39.3169	175.5143	1437.1	0.971	4.92 ± 0.26	1.93 ± 0.07	183 ± 12	4.82 ± 0.27	14.21 ± 0.73
MD-PD063	39.3168	175.5146	1434.8	0.991	4.00 ± 0.22	2.19 ± 0.09	131 ± 9	3.88 ± 0.23	11.45 ± 0.62
MF-PD064	39.3167	175.5146	1433.8	0.987	4.08 ± 0.22	1.65 ± 0.07	178 ± 12	3.99 ± 0.22	11.80 ± 0.61
MF-PD065	39.3167	175.5147	1433.3	0.988	4.47 ± 0.24	1.79 ± 0.08	180 ± 13	4.37 ± 0.25	12.80 ± 0.70
Eruption age of MF: 12.6 ± 3.5 ka INT 2σ : 2.5 ka									

Table 2: Continued.

Sample	Latitude (S)	Longitude (E)	Elevation (MSL)	Shielding factor	$^3\text{He}_{\text{tot}} \pm 1\sigma$ (10^6 at/g)	$^4\text{He}_{\text{tot}} \pm 1\sigma$ (10^{10} at/g)	Total $^3\text{He}/^4\text{He}$ (R/Ra)	$^3\text{He}_{\text{cos}} \pm 1\sigma$ (10^6 at/g)	Exposure age $\pm 1\sigma$ (ka)
NR - Ngā Rimutāmaka flow			<i>Makotuku Member</i>						
NR-PD053	39.3381	175.5873	1369.8	0.996	16.08 ± 0.67	2.46 ± 0.08	474 ± 25	16.05 ± 0.67	46.60 ± 2.12
NR-PD054	39.3384	175.5880	1372.9	1.000	15.34 ± 0.63	1.89 ± 0.07	582 ± 31	15.21 ± 0.64	43.38 ± 1.75
NR-PD055	39.3384	175.5879	1372.7	0.999	14.63 ± 0.62	1.79 ± 0.08	587 ± 35	14.52 ± 0.62	41.41 ± 1.53
NR-PD057	39.3384	175.5880	1372.6	0.995	14.80 ± 0.62	2.61 ± 0.10	408 ± 23	14.67 ± 0.63	42.11 ± 1.63
<i>Eruption age of NR: 42.9 ± 8.6 ka INT 2σ: 1.7 ka</i>									
MA - Makahikatoa flow			<i>Makotuku Member</i>						
MA-PD058	39.3125	175.6116	1594.8	0.996	20.03 ± 0.83	4.82 ± 0.15	299 ± 15	19.75 ± 0.84	48.96 ± 2.60
MA-PD059	39.3125	175.6116	1593.4	0.998	24.08 ± 1.18	9.56 ± 0.27	181 ± 10	23.58 ± 1.21	58.98 ± 2.84
<i>Minimum eruption age of MA: 54.0 ± 18.0 ka INT 2σ: 14.2 ka</i>									
GR - Girdlestone Ridge flow			<i>Mangaehuehu Member</i>						
GR-PD022 (OI)	39.3072	175.5613	2148.0	0.996	7.88 ± 0.21	1.24 ± 0.10	457 ± 37	7.79 ± 0.21	14.02 ± 0.35
GR-PD023 (OI)	39.3074	175.5615	2147.3	0.921	7.61 ± 0.49	1.19 ± 0.13	460 ± 59	7.54 ± 0.49	14.46 ± 0.85
GR-PD024 (OI)	39.3074	175.5616	2145.4	0.990	6.19 ± 0.39	1.28 ± 0.07	348 ± 30	6.12 ± 0.39	$11.11 \pm 0.64^*$
GR-PD025 (OI)	39.3078	175.5615	2128.1	0.993	3.61 ± 0.25	1.87 ± 0.10	139 ± 12	3.50 ± 0.25	$6.81 \pm 0.41^*$
<i>Minimum eruption age of GR: 14.2 ± 2.7 ka INT 2σ: 0.6 ka</i>									

$^3\text{He}_{\text{cos}}$ values were calculated using Equation 3, with magmatic $^3\text{He}/^4\text{He}$ of $5.9 \pm 2.6 \times 10^{-6}$ ($\sim 4.2 \pm 1.9$ Ra). Individual samples are informed with 1σ for reproducibility using the CREp online calculator. Summary eruption age uncertainties represent 2σ values including production rate errors. Internal (INT) 2σ errors do not include production rate errors. All analysed samples consisted of pure pyroxenes with the exception of the site GR, where analysed crystals were olivines with subordinate pyroxenes. For complete data and corrections, see Table A3. Outliers are marked with * after the calculated exposure age. Two aliquots were measured for samples RTm-PD046 and CTb-PD234, for which we calculated a weighted mean of the $^3\text{He}_{\text{cos}}$ as a sample summary.

5 Discussion

5.1 Comparison with previous age constraints

The new Holocene ^3He exposure ages yield eruption ages with higher precision than $^{40}\text{Ar}/^{39}\text{Ar}$ dates of Conway et al. (2016) for this time range (Figure 5). Additionally, young (<20 ka) $^{40}\text{Ar}/^{39}\text{Ar}$ ages of individual samples have normally weak isochrons, as the R values for their linear fits used to calculate crystallization age (released $^{40}\text{Ar}/^{36}\text{Ar}$ vs $^{39}\text{Ar}/^{36}\text{Ar}$ in increasing temperature steps) tend to be relatively low (e.g., Harpel et al., 2004; Conway et al., 2016; Preece et al., 2018). Therefore, young $^{40}\text{Ar}/^{39}\text{Ar}$ ages are very susceptible to the decisions involved in the selection of steps included (or discarded) in the calculation of weighted mean plateau and isochron ages, and our exposure ages based on multiple samples provide more reliable results.

From the four flows sampled in this study with existing $^{40}\text{Ar}/^{39}\text{Ar}$ dates (Conway et al., 2016), two yield eruption ages agreeing with the radiometric dates (Delta Corner and Tukino Slopes-b flows), and two not only outside the 2σ confidence interval of Conway et al. (2016), but older than the $^{40}\text{Ar}/^{39}\text{Ar}$ ages; the Lava Cascade ($^3\text{He}_{\text{cos}}$: 11.4 ± 2.3 ka; $^{40}\text{Ar}/^{39}\text{Ar}$: 0.8 ± 5.6 ka, Mangatoetoenui flows, Iwikau Member) and the Taranaki Falls ($^3\text{He}_{\text{cos}}$: 14.6 ± 2.9 ka; $^{40}\text{Ar}/^{39}\text{Ar}$: 8.8 ± 2.8 ka) flows. The imprecise nature of the radiometric age of the Lava Cascade flow and its weak isochron, together with the good

agreement between our LC samples and the eruption ages we obtained for the Mangatoetoe flows, leads us to conclude that our eruption age for the Lava Cascade flow is more robust than the date provided by Conway et al. (2016). Based on the good clustering of our results (Table 2), we suggest that our $^3\text{He}_{\text{cos}}$ eruption age better represents the true eruption age of the Taranaki Falls flow. Additionally, our eruption age would explain the rootless nature of the flow (Townsend et al., 2017), as it is older than the flank collapse event that affected the northern summit area of Ruapehu at *ca* 10.5 ka (Eaves et al., 2015) and so also the upper section of the Taranaki Falls flow (Figure 6a).

Our results show, in general, good agreement with the lava flow eruption ages refined by Greve et al. (2016) at Ruapehu (Figure 5). The only exception is the Taranaki Falls flow; the refinement by Greve et al. is based on the $^{40}\text{Ar}/^{39}\text{Ar}$ date of Conway et al. (2016), thus it intrinsically agrees with this age and not with our results. Our $^3\text{He}_{\text{cos}}$ eruption ages for the Delta Corner (7.8 ± 1.5 ka; INT 2σ 0.6 ka), Bruce Road (8.1 ± 2.1 ka; INT 2σ 1.5 ka) and Saddle Cone (9.9 ± 2.0 ka; INT 2σ 0.7 ka) flows match the respective age ranges of 8200–7900, 8800–8500 and 9850–8650 BP provided by Greve et al. (2016). Moreover, these results suggest that it is unlikely that P_3 errors have a significant impact on the accuracy of the eruption ages from this work, which is also supported by the good agreement of the local $^3\text{He}_{\text{cos}}$ production rate calibration test by Eaves et al. (2015) with the worldwide mean production rate used in this study.

Eruption ages obtained for the Rangataua proximal and medial flows (13.6 ± 2.6 and 15.8 ± 3.0 ka, respectively) do not agree with a 12–10 ka constraint suggested by Price et al. (2012) based on tephra stratigraphy (using unpublished data). However, tephra correlation on Ruapehu is complex due to the large number of pyroclastic units emplaced at 20–11 ka and their broad geochemical ranges (Pardo et al., 2012a). Detailed studies (Donoghue et al., 2007) attempted to systematize tephra correlation in this area without success, indicating that the andesitic tephra are highly heterogeneous, displaying wide compositional fluctuations during short time intervals. Hence, our eruption ages are more robust than the estimate of 12–10 ka by Price et al. (2012). The other existing constraint for the Rangataua flows was given by a right lateral moraine of the Mangaehuehu Valley dated at 11–14 ka by Eaves et al. (2019), which was thought to correspond in age to the left lateral moraine overlain by the RTm flow (Figure 4d). Our eruption age of 15.8 ± 0.8 ka (INT 2σ , P_3 errors not considered as the moraines were dated using $^3\text{He}_{\text{cos}}$) suggests that the moraine underlying the Rangataua flows is older than the dated right lateral moraine, rather than its equivalent.

Most of the flows dated in this study lack previous age constraints beyond estimations based on geochemical similarity and geographical proximity to lavas with $^{40}\text{Ar}/^{39}\text{Ar}$ dates. The eruption ages obtained for about half of these flows do not agree with these correlations (Figure 5). Five of them (MN, MS, CTb, MF and GR flows) yield ages younger than any of the dates informed for the units they were correlated to (i.e., Turoa, Makotuku and Mangaehuehu members). This can be explained by a sampling bias of Conway et al. (2016) towards older flows, that are more likely to have exposed their slowly-cooled flow interiors (suitable for $^{40}\text{Ar}/^{39}\text{Ar}$ dating) due to their longer periods exposed to erosive processes and the presence of collapsed thick margins in the case of previously ice-impounded flows (Conway et al., 2015). PR and MA deposits are relatively isolated (Figure 4a, b), so the previous geochemical correlations are weaker. The age previously assigned to the PR deposits (Table 1) was, unlike any other lava in this study, based on a correlation with a pyroclastic unit, adding another layer of uncertainty.

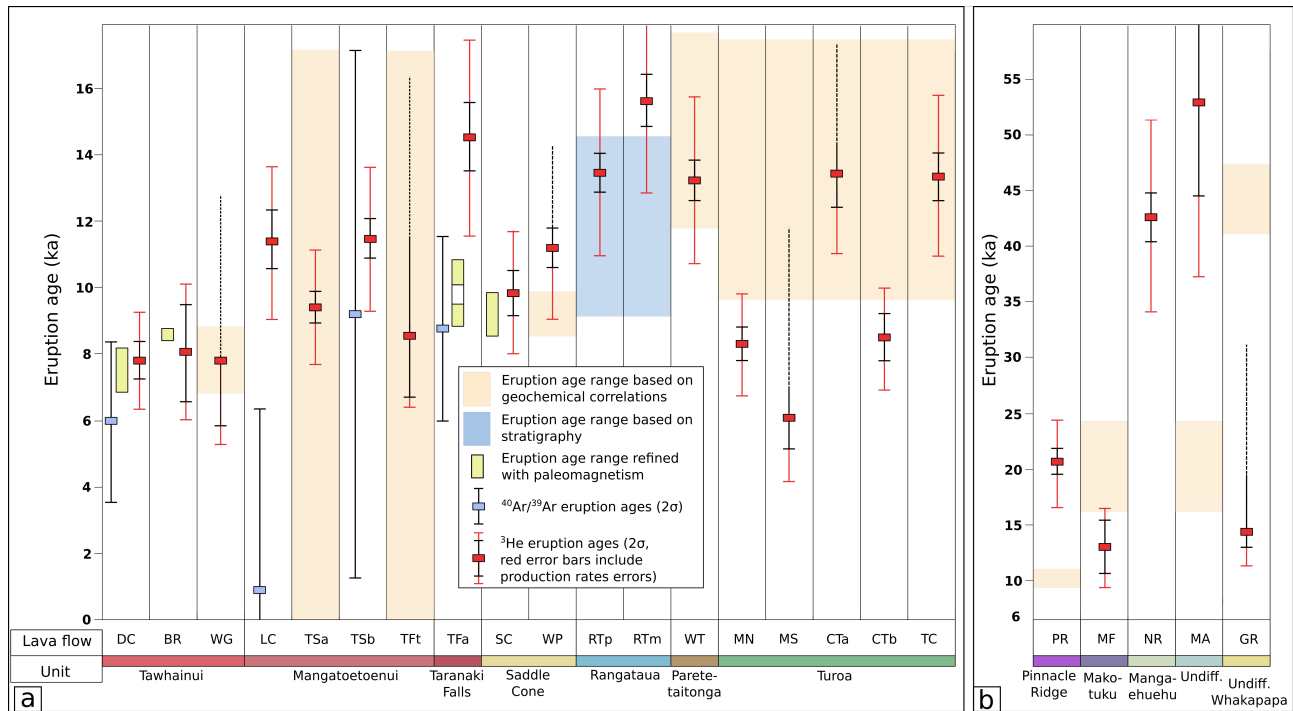


Figure 5. Comparison between eruption ages obtain in this study and previous chronological constraints of the sampled flows. Unit colours correspond to the colours on Figure 1. a) Lavas <20 ka. b) Lava flows that are —or were thought to be— older than 20 ka.

Our results represent the first dates for lavas at the the PR and MA sites and indicate older eruption ages than suggested by geochemical correlations.

5.2 Inconsistency with previous unit classification

Most of the eruption ages measured in this study are consistent with the age and geochemical ranges of the units to which they were assigned by Townsend et al. (2017). Here, we discuss the results we obtained which do not agree with the existing classification.

- Donoghue et al. (1999) linked the Pinnacle Ridge spatter-fed lava with the Taurewa pyroclastic unit (*ca* 10 ka) based on geochemistry and the concentric nature of the isopachs of the Taurewa deposits around the location of PR. Our results indicate that the Pinnacle Ridge deposit was emplaced at 20.4 ± 4.0 ka, during the LGM and *ca* 10 kyr prior to the Taurewa eruptive event, which is consistent with the lack of preservation of a proximal vent, likely associated with a significant erosive period and the retreat of large ice masses. Hence, our eruption age for Pinnacle Ridge suggests that this unit should be included as part of the Mangawhero Formation (50–15 ka) instead of the Whakapapa Formation (<15 ka).

- 565 – MF samples were taken from a large flow considered to be part of the Makotuku Member of the Mangawhero Formation (*ca* 24–16 ka, Table 1) based on its geochemistry. Our results show that this lava flow was erupted at 12.6 ± 3.5 ka, which suggests that, based on age criteria, it could be classified as part of the Whakapapa Formation (<15 ka).
- Our NR site was mapped as part of the Makotuku Member, on an area dominated by outcrops of Mangaehuehu lavas (Figure 4d). Our eruption age of 42.9 ± 8.6 ka for this site, together with the geochemical similarity of the NR samples to Mangaehuehu lavas (47–40 ka, Conway et al., 2016, see Table 1), suggests that the sampled outcrop is part of the Mangaehuehu Member.
- 570 – The outcrop we collected the MA samples from has, due to its geochemical similarity, been considered part of the Makotuku Member. Two exposure ages indicate that the Makahikatoa flow was emplaced at, or prior to, 50 ka, suggesting that it was formed during the first eruptive stages of the Mangawhero or in the late stages of the Waihianoa Formation (see Table 1), with a geochemical signature common in lavas emplaced at 24–16 ka.
- 575 – Exposure ages of GR samples (previously mapped as part of the Mangaehuehu Member) suggest that this lava was emplaced during the last 15 kyr, which is inconsistent with it being part of the Mangawhero Formation. However, its geochemistry differentiates this outcrop from the rest of the Whakapapa lavas (Conway et al., 2016), thus it is likely to be part of a new member within the Whakapapa Formation.
- 580 – The results we obtained for flows from the Turoa Member indicate that lava was emplaced on Ruapehu’s western flanks at *ca* 15–12 ka (Turoa Cascades and Central Turoa-a flows, as well as data from Conway et al., 2016) and, after a hiatus of ~4 kyr, again at around 8 ka (Mangaturuturu North and Central Turoa-b flows). Thus, we suggest the extension of the younger limit of the Turoa Member to 8 ka. Similarly, the obtained eruption ages redefine the age limits of the Rangataua Member (17–12 ka), Saddle Cone Member (12–8.5 ka), Taranaki Falls flow (16–13 ka) and Mangatoetoenui flows (12–9 ka).
- 585

5.3 Postglacial effusive activity of Ruapehu

Our $^3\text{He}_{\text{cos}}$ based eruption ages allow two periods of enhanced effusive activity since the LGM to be identified on Ruapehu (17–12 ka, Figure 6a and b; and 9–7.5 ka, Figure 6e), during which lava emplacement on different areas of the volcano occurred nearly simultaneously.

- 590 Our results show that, during the last glacial termination (*ca* 17–14 ka; Figure 6a), effusive activity affected the southern (Rangataua medial and, likely, the immense distal Rangataua flows of $>1.5 \text{ km}^3$) and northern (Taranaki Falls flow) slopes of Ruapehu, suggesting that its southern and northern vents were active during this period. Radiometric dates published by Conway et al. (2016, see Table 1) suggest that, during this period, lava flows were also emplaced on Ruapehu’s western (15.1 ± 2.4 ka, Turoa Member) and northwestern (14.8 ± 3.0 ka, Paretaitonga Member) flanks. This period of generalized activity across Ruapehu continued until *ca* 12 ka (Figure 6b), with increasing intensity on the western flanks and decreasing intensity on the southern flanks. Eruption ages of the Whakapapa (13.3 \pm 0.7 ka), Turoa Cascades (13.4 \pm 0.7 ka) and Rangataua
- 595

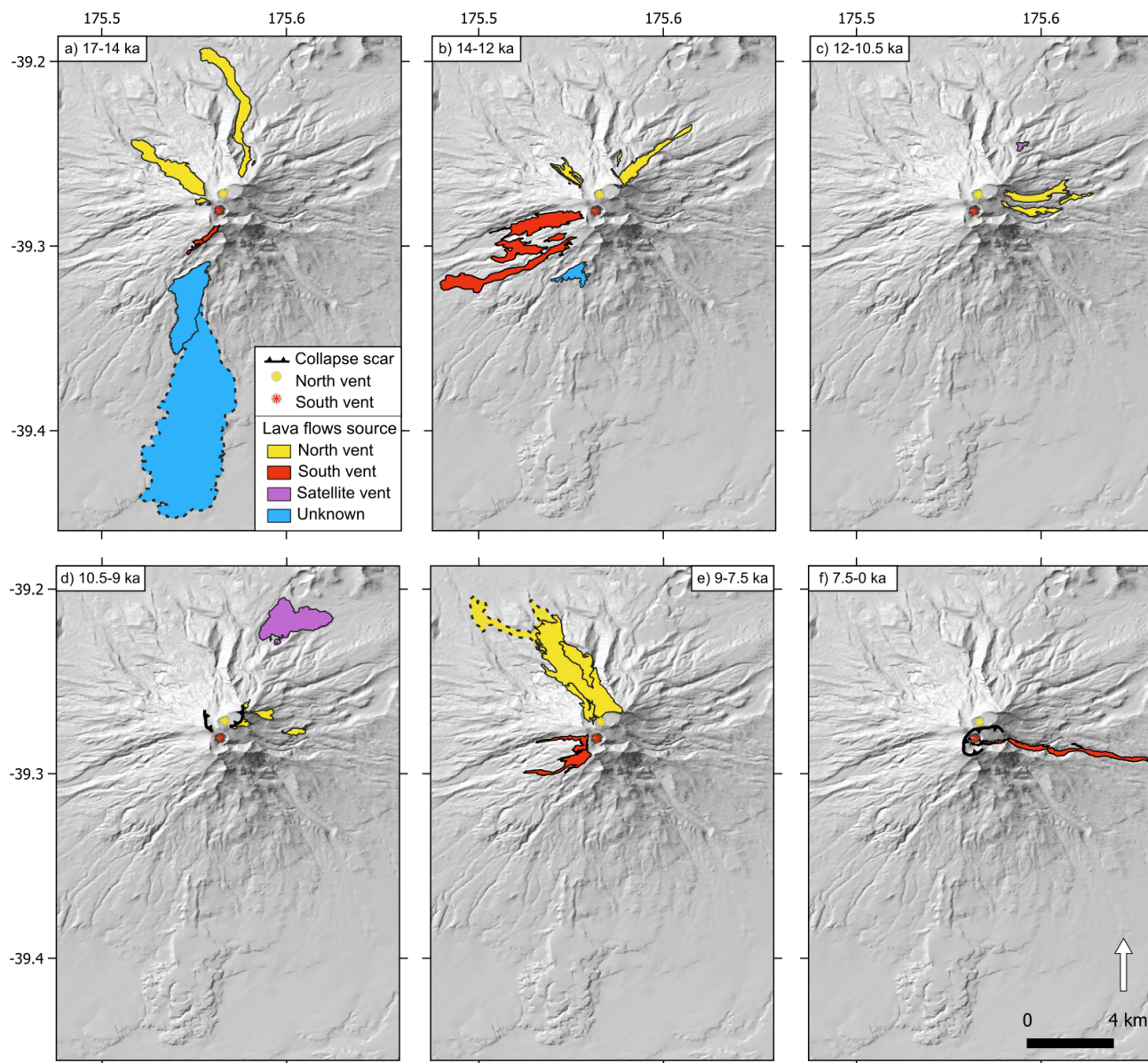


Figure 6. Lava flows emplaced at Ruapehu through time after the LGM. Collapse scars corresponds to flank collapse episodes at (d) 10.4–10.6 cal ka BP (Palmer and Neall, 1989; Eaves et al., 2015, Murimotu debris avalanche) and at (f) ca 4.6 ka, (Mangaio Formation, Donoghue, 1991; Donoghue and Neall, 2001). Lava flows with dotted boundaries in (a) and (e) have not been dated; their ages have been assigned based on geochemical and geomorphological similarities with dated flows.

proximal (13.6 ± 0.6 ka) flows are nearly identical, indicating that lava emplacement occurred nearly simultaneously on different flanks of the volcanic edifice. In the early Holocene (i.e. 12–10.5 ka, Figure 6c), activity was focused on the east and northeast of the volcano, generating the first lavas of the Mangatoetoenui flows, as well as lavas emerging from satellite vents (Waihohonu Plateau flow). After a flank collapse that affected part of the northern edifice at *ca* 10.5 ka (Eaves et al., 2015), lava flows continued to be emplaced on the eastern flanks from the northern vent and erupting from satellite vents on the northeast in short time lapses (<2 kyr), generating the large Saddle Cone flow (Figure 6d). The rate of lava production (i.e. amount of individual lava flows produced) between 9 and 7.5 ka (Figure 6e) was likely to have been the highest in the last 20 kyr at Ruapehu. Our results suggest that, during this time, most of the flows forming the Tawhainui sequence on north Ruapehu were emplaced from the northern vent, filling a topographic low left by the flank collapse. At a similar time, the last lavas of the Turoa Member (Mangaturuturu North and, Central Turoa-b flows) were being erupted from the southern vent and flowed to the west of the edifice. Effusive activity then declined, and after another episode of flank collapse that modified the topography surrounding the summit southern vent, lava flow emplacement was confined to the current outlet of Ruapehu's crater lake and flowed to the east (Whangaehu valley, Figure 6f) at 2400–2050 BP (Greve et al., 2016).

Between ~23 and ~10 ka, Ruapehu produced at least five plinian eruptions (as well as dozens of smaller explosive events) sourced from its northern vent (Pardo et al., 2012b). In contrast, effusive activity occurred from both the southern and northern vents until ~8 ka. Lack of high-resolution ages of the pyroclastic deposits, however, hinder our ability to compare precisely the timing of these events. After this period of enhanced volcanism (finishing at ~10 ka for explosive, Pardo et al., 2012b, and at ~8 ka for effusive events), activity at Ruapehu decreased significantly in magnitude and was restricted to the southern vent. However, our data exposes time intervals during the last 17 ka when lavas have been emplaced from both Ruapehu's summit vents, challenging the assumption that volcanic hazards should be expected from the southern but not from the northern vent (e.g., Keys and Green, 2010; Leonard et al., 2021).

5.4 Applicability of cosmogenic ^3He dating on stratovolcanoes

This study represents the first large-scale application of $^3\text{He}_{\text{cos}}$ as a dating tool for lava flows at stratovolcanoes. We provide $^3\text{He}_{\text{cos}}$ -based eruption age constraints for 20 young lava flows at Ruapehu, contributing to a detailed lava flow eruptive history for Ruapehu during the last 20 kyr (subsection 5.3). Our data has good intra-flow clustering, inter-flow consistency, and good agreement with previous chronological constraints, demonstrating that robust eruption ages can be obtained for lava flows using $^3\text{He}_{\text{cos}}$ not only for basaltic lavas (e.g., Kurz et al., 1990; Licciardi et al., 2007; Foeken et al., 2009; Marchetti et al., 2014; Medynski et al., 2015), but also for andesitic lavas at stratovolcanoes.

Analyses of our samples yielded low $^4\text{He}_{\text{tot}}$ values (likely influenced by repeated HF leaching steps of the pyroxenes during sample preparation, Bromley et al., 2014) and low concentrations of radioactive elements (as expected from samples of intermediate compositions), which in turn resulted in small non-cosmogenic corrections and, added to analytical errors, small internal uncertainties of the obtained exposure ages. Like most other $^3\text{He}_{\text{cos}}$ -based ages, however, the $^3\text{He}_{\text{cos}}$ production rate uncertainty makes the largest contribution to our errors, imparting an uncertainty of ~10% to all calculated ages, which points

630 out that more high-quality calibration sites are required to reduce these uncertainties and improve the quality of ^3He -based exposure ages (Blard, 2021).

Considering these sources of uncertainties, our data shows that the resolution of $^3\text{He}_{\text{cos}}$ -based eruption ages can be higher than $^{40}\text{Ar}/^{39}\text{Ar}$ or K/Ar for young intermediate lavas (see Figure 5). In older lava flows (>20 ka), radiometric methods can resolve emplacement ages more precisely (e.g., Lanphere, 2000; Harpel et al., 2004; Conway et al., 2016), whereas cosmogenic exposure ages become less certain due to production rate errors. Consequently, cosmogenic nuclides exposure dating has the potential to yield better results compared to $^{40}\text{Ar}/^{39}\text{Ar}$ or K/Ar when dating post-LGM ka lava flows (e.g., Harpel et al., 2004; Parmelee et al., 2015; Conway et al., 2016; Alcalá-Reygosa et al., 2018), and offers a valid alternative to date older lavas when no radiometric dating method can be applied (e.g. the site NR from this study, which ages match with higher-precision $^{40}\text{Ar}/^{39}\text{Ar}$ dates of geochemically similar lavas). Additionally, young lava flows are more likely to have original lava surfaces preserved, as they were exposed to erosive and/or depositional processes for a relatively limited time. For the same reason, they are less likely to have exposed flow interiors needed for $^{40}\text{Ar}/^{39}\text{Ar}$ or K/Ar dating (Calvert and Lanphere, 2006; Fierstein et al., 2011), which makes $^3\text{He}_{\text{cos}}$ dating an ideal supplementary technique to radiometric methods when dating young pyroxene- and olivine-bearing lavas both at basaltic volcanic areas and andesitic stratovolcanoes.

6 Conclusions

645 We analysed pyroxene- and olivine-hosted $^3\text{He}_{\text{cos}}$ in 77 samples from 23 lava flows on Ruapehu volcano, Aotearoa New Zealand, and obtained 16 eruption ages (between 7.8 ± 0.6 and 42.9 ± 1.7 ka; analytical 2σ) and seven minimum eruption ages, refining the chronology of lava flow emplacement at Ruapehu in the last 20 kyr.

Our data expose that weak $^{40}\text{Ar}/^{39}\text{Ar}$ isochrons led to unreliable eruption ages for two postglacial lavas at Ruapehu, and stress the necessity of robust age constraints when using paleomagnetism as an age-refining tool.

650 Our results show effusive activity at Ruapehu occurred from different vents during the last 17 kyr, affecting various sectors of the volcanic edifice over short time intervals. Based on our observations, we propose that the number of effusive eruptions during the last 20 kyr peaked at 17–12 and 9–7.5 ka. This represents a significant contribution to the hazard database of Aotearoa New Zealand, and valuable data for investigating temporal links of volcanic activity in the Tāupo Volcanic Zone.

Cosmogenic nuclides exposure dating can provide greater detail on the recent effusive chronology of statovolcanoes, filling the gap left by the low resolution and challenges in acquiring adequate samples for radiometric dating of young lava flows.

Data availability. All used data is available in the supplementary file S4 and appendix table A2.

Abbreviation	Lava Flow Name	Area
BR	Bruce Road	North
CTa	Central Turoa-a	West
CTb	Central Turoa-b	West
DC	Delta Corner	North
GR	Girdlestone Ridge	South
LC	Lava Cascade	East
MA	Makahikatoa	Southeast
MF	Makotuku Flat	West
MN	Mangaturuturu North	West
MS	Mangaturuturu South	West
NR	Ngā Rimutāmaka	South
PR	Pinnacle Ridge	North
RTm	Rangataua medial	South
RTp	Rangataua proximal	South
SC	Saddle Cone	Northeast
SCw	Saddle Cone - western lobe	Northeast
SCe	Saddle Cone - eastern lobe	Northeast
TC	Turoa Cascades	West
TFa	Taranaki Falls	North
TFt	Tukino Flats	East
TSa	Tukino Slopes-a	East
TSb	Tukino Slopes-b	East
WG	Whakapapa Glacier	North
WP	Waihohonu Plateau	Northeast
WT	Whakapapaiti	Northwest

Table A1. Abbreviations list, used for sampling sites and samples.

Table A2. Normalized major and trace elements of bulk rock and analysed minerals for each sampled lava flow.

Bulk rock		normalized wt. %												ppm									
Site	SiO ₂	Al ₂ O ₃	Fe ₂ O ₃	MnO	MgO	CaO	Na ₂ O	K ₂ O	TiO ₂	P ₂ O ₅	LOI	Maj _{tot}	Li	B	Cr	Co	Ni	Gd	Sm	U	Th		
DC	57.01	15.88	8.23	0.13	5.37	7.42	3.14	1.40	0.68	0.18	0.56	99.26	17.9	20.0	85.19	26.68	45.59	2.69	2.75	1.08	4.04		
BR	55.80	16.49	7.69	0.12	4.74	6.38	3.11	1.55	0.68	0.14	3.31	100.23	20.4	22.8	101.82	23.64	40.78	2.79	2.83	1.30	4.91		
WG	54.87	16.02	9.25	0.13	5.34	6.59	2.92	1.41	0.72	0.14	2.62	99.46	17.6	20.1	91.32	26.95	45.80	2.75	2.75	1.13	4.36		
LC	52.61	18.94	8.79	0.13	4.21	5.18	2.65	1.52	0.78	0.15	5.04	99.79	19.6	20.5	64.56	21.82	20.55	2.87	2.84	1.46	5.22		
TSa	53.97	17.20	8.91	0.13	4.36	6.51	2.81	1.41	0.79	0.16	3.76	99.52	16.3	19.6	45.17	22.39	14.11	2.79	2.81	1.19	4.79		
TSb	52.75	18.33	8.68	0.13	4.62	5.87	2.64	1.42	0.77	0.14	4.65	100.47	19.0	20.0	85.21	24.29	24.85	2.79	2.76	1.42	5.03		
TFt	55.98	17.28	8.40	0.13	4.26	6.59	2.94	1.42	0.75	0.13	2.11	100.05	17.2	21.2	56.97	21.95	18.92	2.61	2.57	1.23	4.61		
TFa	57.17	16.80	7.81	0.12	4.09	6.88	3.15	1.52	0.72	0.13	1.61	100.25	16.8	22.3	60.99	20.34	19.91	2.91	2.96	1.34	5.09		
SC	56.76	16.48	7.88	0.12	4.64	7.02	3.07	1.52	0.72	0.15	1.63	99.87	21.3	21.7	86.23	23.75	31.36	2.77	2.81	1.32	4.92		
WP	55.42	16.60	8.13	0.12	4.87	6.58	2.77	1.31	0.70	0.13	3.37	100.04	18.8	20.3	95.47	24.80	36.95	2.72	2.60	1.18	4.49		
PR	58.59	16.12	6.78	0.10	4.42	5.69	3.04	1.79	0.65	0.14	2.68	100.29	22.5	21.9	183.67	20.39	53.61	2.57	2.50	1.45	5.50		
RTp	56.56	17.39	7.60	0.12	3.37	5.35	3.15	1.74	0.75	0.15	3.84	99.83	19.2	23.9	36.93	16.88	12.67	3.00	3.11	1.49	5.91		
RTm	56.64	16.82	7.67	0.12	3.57	5.72	3.15	1.69	0.75	0.21	3.67	99.53	18.6	23.4	40.90	17.75	13.20	3.15	3.17	1.53	6.03		
WT	55.32	17.34	8.29	0.12	4.19	5.79	2.85	1.52	0.76	0.14	3.69	100.24	20.3	20.9	57.45	20.84	18.59	2.76	2.80	1.32	5.40		
MN	53.66	17.72	8.07	0.12	5.01	6.09	2.93	1.47	0.66	0.13	4.14	100.44	19.2	22.5	93.87	25.17	47.08	2.42	2.41	1.34	4.86		
MS	55.58	15.71	9.54	0.13	4.51	6.18	2.87	1.49	0.84	0.13	3.01	100.20	13.8	19.2	54.80	23.51	17.53	2.45	2.45	0.94	4.99		
CTa	56.67	16.49	8.12	0.12	4.36	6.49	3.01	1.50	0.72	0.15	2.37	99.64	20.2	21.8	88.79	22.15	29.15	2.75	2.80	1.35	5.02		
CTb	56.01	16.78	8.32	0.12	4.60	7.12	3.01	1.39	0.74	0.13	1.77	99.29	19.3	20.8	89.86	23.46	27.88	2.72	2.75	1.20	4.51		
TC	56.18	16.49	8.44	0.13	4.60	7.03	3.06	1.48	0.78	0.14	1.66	99.90	17.3	20.0	71.52	22.48	18.63	2.96	2.95	1.22	4.71		
MF	58.67	16.98	6.52	0.093	2.96	5.91	3.50	1.87	0.84	0.16	2.50	100.13	26.8	27.3	49.22	16.60	18.75	2.96	3.13	1.63	6.12		
NR	57.92	14.71	6.81	0.11	6.24	5.96	2.96	1.85	0.73	0.19	2.53	99.77	29.7	23.4	308.14	25.08	109.34	3.14	3.25	1.74	6.50		
MA	58.73	17.28	6.77	0.10	3.09	5.26	3.29	1.55	0.68	0.13	3.12	99.82	21.0	24.4	34.02	17.42	14.05	2.77	2.85	1.31	5.00		
GR	55.76	15.21	7.40	0.12	6.09	6.77	2.80	1.35	0.66	0.14	3.71	100.13	20.4	20.7	215.77	26.79	73.65	2.71	2.78	1.14	4.50		
Minerals																							
DC	52.11	1.58	20.53	0.41	22.11	4.08	0.09	<DL	0.31	<DL	-1.20	99.63	<2	10.7	285.89	98.63	187.40	1.07	0.78	0.01	0.040		
BR	51.76	1.97	18.03	0.36	19.70	8.31	0.20	0.04	0.39	<DL	-0.76	99.55	<2	8.59	398.47	85.29	172.81	2.37	1.97	0.04	0.144		
WG	51.71	1.61	20.15	0.39	21.71	4.76	0.10	<DL	0.34	<DL	-0.77	99.85	<2	12.8	371.23	92.22	182.44	1.38	1.08	0.01	0.048		
LC	51.54	1.59	20.41	0.43	20.50	5.74	0.12	<DL	0.39	<DL	-0.71	99.32	<2	10.7	337.72	85.76	129.55	1.97	1.60	0.02	0.056		
TSa	49.38	1.51	24.99	0.44	21.19	2.14	0.05	<DL	0.86	<DL	-0.57	99.83	<2	7.35	404.65	98.37	143.62	0.65	0.44	0.02	0.052		
TSb	51.60	1.52	21.23	0.45	21.34	4.16	0.08	<DL	0.37	<DL	-0.76	100.32	<2	10.9	277.49	88.05	117.96	1.39	1.08	0.01	0.050		
TFt	51.18	1.53	21.60	0.45	20.94	4.64	0.09	<DL	0.49	<DL	-0.90	99.54	<2	16.7	279.53	88.18	120.06	1.59	1.27	0.01	0.047		
TFa	51.27	1.51	20.55	0.42	20.94	5.09	0.10	<DL	0.40	<DL	-0.28	99.10	<2	11.0	367.38	85.09	130.22	1.65	1.35	0.02	0.062		
SC	51.41	1.91	19.70	0.39	19.54	7.18	0.18	0.04	0.42	<DL	-0.78	100.00	<2	9.17	394.61	80.89	127.03	2.56	2.07	0.05	0.185		
WP	52.19	2.37	16.91	0.33	19.95	8.16	0.28	0.10	0.38	<DL	-0.67	99.86	<2	10.2	645.87	77.50	164.79	2.21	1.80	0.10	0.358		
PR	51.05	2.01	20.06	0.39	20.02	6.31	0.13	<DL	0.41	<DL	-0.39	99.57	<2	31.0	632.12	83.14	163.52	1.94	1.54	0.03	0.141		
RTp	51.08	1.50	22.65	0.43	21.53	3.04	0.07	<DL	0.49	<DL	-0.80	100.29	<2	5.71	405.44	91.30	153.24	1.06	0.80	0.01	0.049		
RTm	51.38	1.46	23.10	0.44	21.71	2.91	0.06	<DL	0.47	<DL	-1.53	99.84	<2	7.48	321.50	91.05	135.00	1.07	0.82	0.01	0.045		
WT	47.28	1.59	26.88	0.43	20.27	2.90	0.06	<DL	1.41	<DL	-0.82	99.76	<2	10.7	465.85	96.87	142.07	0.89	0.68	0.03	0.069		
MN	52.02	1.51	21.69	0.43	22.68	2.47	0.06	<DL	0.31	<DL	-1.18	99.37	<2	13.4	269.95	102.76	196.34	0.66	0.46	0.01	0.040		
MS	51.76	1.62	20.40	0.42	21.30	5.00	0.10	<DL	0.38	<DL	-0.97	99.36	<2	23.6	374.34	88.31	122.86	1.52	1.20	0.01	0.046		
CTa	51.45	1.64	20.05	0.41	20.42	5.92	0.13	<DL	0.38	<DL	-0.40	99.89	<2	9.23	409.65	84.51	143.50	2.11	1.72	0.03	0.098		
CTb	51.08	1.63	20.86	0.41	20.43	5.87	0.12	<DL	0.62	<DL	-1.03	99.35	<2	10.8	410.51	84.63	144.39	2.03	1.67	0.02	0.065		
TC	51.56	1.62	20.37	0.41	21.10	5.02	0.10	<DL	0.35	<DL	-0.53	100.21	<2	8.01	391.62	88.11	124.68	1.51	1.19	0.01	0.046		
MF	50.94	1.66	22.07	0.39	21.93	3.35	0.07	<DL	0.82	<DL	-1.22	99.65	<2	13.6	475.60	95.40	181.14	0.94	0.73	0.02	0.058		
NR	52.64	1.95	16.10	0.28	22.62	6.82	0.15	<DL	0.35	<DL	-0.90	99.71	<2	11.7	1184.21	83.92	352.04	1.56	1.27	0.02	0.042		
MA	49.70	2.03	22.77	0.39	21.09	3.88	0.08	<DL	0.89	<DL	-0.83	99.44	<2	17.7	332.48	92.02	106.83	0.88	0.64	0.02	0.081		
GR	54.07	1.52	13.92	0.27	27.48	2.89	0.05	<DL	0.19	<DL	-0.39	99.30	<5	6.22	1649.09	87.13	360.96	0.36	0.26	<DL	0.022		

Detection limits (DL) are 0.03 wt.% for K₂O; 0.10 wt.% for P₂O₅; 2 ppm for B; and 0.01 ppm for U.

Table A3: Sample data used to compute exposure ages.

Sample	Latitude (S)	Longitude (E)	Elevation (MSL)	Surface dip (°)	Dip direction (°)	Shielding factor	Density (g/cm ³)	Thickness (cm)	P _{nuc} (10 ² at/g/yr)	Closure age (Ma)	H _{enuc} (at)	P ₃ (at/g/yr)	P ₄ (10 ⁵ at/g/yr)	R factor
SC-PD001	39.2143	175.6011	1439.0	-	-	0.998	1.89	3.6	406	0.010	406	231.22	3.13	0.9932
SC-PD002	39.2143	175.6010	1439.3	-	-	0.998	2.01	3.2				245.83		0.9932
SC-PD003	39.2146	175.5997	1443.3	-	-	0.998	2.01	2.4				245.86		0.9932
WP-PD007	39.2479	175.5882	1911.7	10	190	0.996	2.13	3.3	414	0.010	415	487.90	6.08	0.9906
WP 008	39.2479	175.5882	1912.1	18	30	0.995	2.06	3.0				487.90		0.9906
BR-PD014	39.2201	175.5406	1360.0	-	-	0.999	2.15	2.7	565	0.010	565	317.93	0.75	0.9982
BR-PD016	39.2198	175.5379	1359.2	28	55	0.981	2.32	2.6				320.37		0.9982
BR-PD017	39.2190	175.5409	1332.6	-	-	0.998	2.25	2.7				313.04		0.9982
BR-PD018	39.2190	175.5411	1332.4	-	-	0.998	2.15	4.3				317.93		0.9982
GR-PD022	39.3072	175.5613	2148.0	-	-	0.996	2.15	2.7	254	0.020	508	589.39	0.44	0.9994
GR-PD023	39.3072	175.5615	2147.2	45	180	0.921	2.24	4.5				584.50		0.9994
GR-PD024	39.3074	175.5616	2145.4	-	-	0.990	2.18	4.6				574.72		0.9994
GR-PD025	39.3078	175.5615	2128.1	-	-	0.993	2.80	4.7				539.25		0.9994
RT-PD027	39.3140	175.5509	1831.4	-	-	0.997	1.84*	5.5	296	0.015	444	468.33	0.74	0.9988
RT-PD028	39.3140	175.5509	1833.1	-	-	0.996	1.79	5.3				467.11		0.9988
RT 029	39.3140	175.5509	1832.9	-	-	0.996	1.84*	5.3				469.56		0.9988
RT-PD030	39.3143	175.5512	1816.4	20	230	0.988	1.89	5.1				465.89		0.9988
RT-PD045	39.3234	175.5520	1585.9	20	80	0.991	2.80	4.2	401	0.015	601	399.86	0.75	0.9986
RT-PD046	39.3249	175.5508	1567.6	29	145	0.979	2.07	3.6				393.74		0.9986
RT-PD047	39.3251	175.5503	1567.4	-	-	0.997	2.27	3.0				392.52		0.9986
RT-PD048	39.3250	175.5503	1567.3	-	-	0.997	2.19	3.4				374.18		0.9985
NR-PD053	39.3381	175.5873	1369.8	15	3	0.996	2.39	4.8	654	0.045	2944	359.50	1.01	0.9979
NR-PD054	39.3384	175.5880	1372.9	-	-	1.000	2.06	4.2				360.73		0.9979
NR-PD055	39.3384	175.5879	1372.5	-	-	0.999	2.15	3.2				358.28		0.9979
NR-PD057	39.3384	175.5880	1372.6	-	-	0.995	2.47	3.5				359.50		0.9979
MA-PD058	39.3125	175.6116	1570.7	14	190	0.996	2.45	2.9	818	0.050	4089	414.53	1.29	0.9977
MA-PD059	39.3125	175.6116	1569.3	-	-	0.998	2.21	3.20				408.42		0.9976
MF-PD061	39.3169	175.5143	1437.0	-	-	0.971	2.15	3.0	729	0.013	948	353.39	1.14	0.9975
MF-PD063	39.3168	175.5146	1434.8	-	-	0.991	1.81	3.8				348.50		0.9975
MF-PD064	39.3167	175.5146	1433.8	-	-	0.987	1.95	3.6				349.72		0.9975
MF-PD065	39.3167	175.5147	1433.3	11	180	0.988	1.80	2.6				350.94		0.9975
TC-PD066	39.3014	175.5193	1533.2	-	-	0.997	2.17	6.2	292	0.013	380	375.40	7.59	0.9985
TC-PD067	39.3015	175.5192	1533.6	-	-	0.997	2.11	4.5				379.07		0.9985
TC-PD068	39.3015	175.5192	1533.1	-	-	0.997	2.15	7.4				377.85		0.9985
TC-PD070	39.3012	175.5193	1528.0	-	-	0.997	1.99	4.3				376.62		0.9985
WT-PD073	39.2569	175.5428	1892.4	20	260	0.987	2.09	3.5	493	0.013	641	468.33	0.77	0.9984
WT-PD074	39.2569	175.5428	1892.1	-	-	0.988	2.22	3.8				471.99		0.9984
WT-PD075	39.2560	175.5397	1891.2	-	-	0.997	2.18	3.3				471.99		0.9984
PR-PD083	39.2370	175.5672	1730.7	16	310	0.979	2.28	3.5	1557	0.020	3115	453.66	2.11	0.9965
PR-PD084	39.2386	175.5689	1860.9	24	180	0.988	2.18	4.7				492.79		0.9968
PR-PD085	39.2385	175.5688	1857.9	16	330	0.997	2.12	4.3				497.68		0.9968
TFa-PD088	39.2067	175.5668	1308.2	-	-	0.999	2.39	3.8	513	0.015	769	321.60	1.17	0.9973
TFa-PD090	39.2060	175.5665	1290.4	16	90	0.996	2.31	5.0				316.71		0.9972
TFa-PD091	39.2059	175.5664	1288.2	-	-	0.999	2.23	4.2				317.93		0.9972
SC-PD093	39.2115	175.6139	1308.2	17	40	0.993	2.30	2.6	537	0.010	537	313.04	3.71	0.9911
TSa-PD205	39.2761	175.6021	1905.0	-	-	0.983	2.12	5.6	305	0.010	305	476.89	1.05	0.9983
TSa-PD206	39.2761	175.6021	1905.9	-	-	0.997	2.21	4.8				480.56		0.9984
TSa-PD207	39.2761	175.6021	1905.5	-	-	0.997	2.37	4.2				481.78		0.9984

Table A3: Continued.

Sample	Latitude (S)	Longitude (E)	Elevation (MSL)	Surface dip (°)	Dip direction (°)	Shielding factor	Density (g/cm ³)	Thickness (cm)	P _{nuc} (10 ² at/g/yr)	Closure age (Ma)	He _{nuc} (at)	P ₃ (at/g/yr)	P ₄ (10 ⁵ at/g/yr)	R factor
TSb-PD209	39.2815	175.5993	1932.5	-	-	0.997	2.20*	2.4	506	0.010	506	494.01	0.75	0.9989
TSb-PD210	39.2815	175.5992	1935.0	17	90	0.989	2.14	2.9				500.13		0.9988
TSb-PD211	39.2816	175.5993	1929.2	20	110	0.993	2.26	3.7				497.68		0.9988
TFt-PD212	39.2726	175.6261	1521.2	-	-	0.994	2.07	5.9	703	0.010	703	359.50	0.76	0.9984
TFt-PD213	39.2726	175.6263	1522.0	10	40	0.998	2.14	6.5				369.29		0.9985
TFt-PD214	39.2723	175.6271	1506.4	-	-	0.988	2.23	6.5				353.39		0.9984
MN-PD217	39.2829	175.5322	1815.9	-	-	0.993	2.11	2.6	623	0.008	498	446.32	0.65	0.9989
MN-PD218	39.2829	175.5321	1813.9	13	220	0.993	2.24	5.2				448.77		0.9989
MN-PD219	39.2829	175.5321	1812.1	-	-	0.993	2.22	4.0				425.53		0.9988
MN-PD220	39.2829	175.5322	1817.5	-	-	0.993	2.06	3.2				449.99		0.9989
MN-PD221	39.2829	175.5325	1822.8	-	-	0.993	2.20	4.0				446.32		0.9989
MS-PD222	39.2845	175.5304	1750.6	36	170	0.955	2.23	5.0	901	0.010	901	414.53	0.76	0.9986
MS-PD223	39.2845	175.5305	1751.4	-	-	0.992	2.41	4.0				412.08		0.9986
MS-PD224	39.2845	175.53005	1750.9	-	-	0.992	2.33	4.1				401.08		0.9986
CTa-PD229	39.2958	175.5395	1924.0	7	300	0.996	1.96	3.2	415	0.015	623	498.90	1.81	0.9972
CTa-PD230	39.2959	175.5396	1925.1	-	-	0.996	2.21	2.9				500.13		0.9973
CTb-PD231	39.2998	175.5392	1877.5	-	-	0.996	2.22	3.4	439	0.008	351	432.87	1.26	0.9978
CTb-PD232	39.3001	175.5390	1873.2	20	190	0.991	2.14	4.1				467.11		0.9979
CTb-PD233	39.3001	175.5390	1872.0	15	240	0.994	2.17*	2.8				465.89		0.9979
CTb-PD234	39.3003	175.5391	1873.4	-	-	0.996	2.15	3.2				467.11		0.9979
LC-PD254	39.2718	175.6052	1827.1	-	-	0.997	2.01	5.4	506	0.010	506	462.22	1.18	0.9981
LC-PD255	39.2718	175.6053	1826.6	-	-	0.997	2.07	6.4				461.00		0.9981
LC-PD256	39.2718	175.6053	1825.6	-	-	0.996	2.08	6.0				452.44		0.9980
LC-PD257	39.2718	175.6053	1824.7	16	330	0.996	2.05	3.7				462.22		0.9981
WG-PD325	39.2557	175.5551	2079.1	21	357	0.991	2.25	4.0	329	0.008	264	536.81	2.45	0.9966
WG-PD326	39.2556	175.5549	2066.7	-	-	0.995	2.30	3.2				520.91		0.9965
DC-PD327	39.2346	175.5515	1600.4	-	-	0.999	2.22	3.5	401	0.008	321	379.07	0.67	0.9987
DC-PD329	39.2342	175.5509	1591.8	-	-	0.999	2.37	4.3				380.29		0.9987
DC-PD330	39.2341	175.5507	1590.3	-	-	0.999	2.21	3.4				377.85		0.9987

Density measures were obtained with the hydrostatic method. Density values marked with * were calculated by averaging densities of other samples from the same site. P_{nuc}, Closure age, He_{nuc}, and P₄ values are considered equal for all samples of the same flow.

Author contributions. TEXT

660 PD carried out field sampling, mineral separation, He isotopes measurements, data processing and interpretation, and manuscript writing. SE assisted with sampling, data processing and manuscript revision. BK did the project supervision, obtained resources and reviewed the manuscript. PB helped with methodology, data analysis and paper revision. AN reviewed and edited the manuscript. GL helped with resources and data interpretation. DT assisted with data interpretation. JC helped with paper revision. CC helped with data interpretation. SB assisted with mineral separation. GF, LZ and BT helped with He isotopes measurements.

Competing interests. TEXT

665 We declare that none of the authors has competing interests.

Acknowledgements. We would like to acknowledge Ngāti Rangi, Uenuku and Ngāti Tūwharetoa Iwi, *tangata whenua* and guardians of Ruapehu. We are grateful to Mark Kurz, David Marchetti and Eric Portenga, whose comments as referees significantly improved the quality of this manuscript. We would also like to thank the Resilience to Nature Challenges (RNC) program, the Australian Institute of Nuclear Science and Engineering (AINSE), Mason Trust, The Royal Society of New Zealand, and The Tongariro Natural History Society for providing 670 funds; the New Zealand's Department of Conservation for sampling permission; Amy Dreyer, Gilles Seropian and Alexander Marshall for assistance in the field; Hollei Gabrielsen for Māori subjects advise and aid with permit process; Chris Grimshaw for help with laboratory procedures; and Mark Henson and Nigel Seebeckfor their help in the Tukino Access Road ford.

References

- Ackert, R. P., Singer, B. S., Guillou, H., Kaplan, M. R., and Kurz, M. D.: Long-term cosmogenic ^3He production rates from $^{40}\text{Ar}/^{39}\text{Ar}$ and K-Ar dated Patagonian lava flows at 47°S , *Earth and Planetary Science Letters*, 210, 119–136, [https://doi.org/10.1016/S0012-821X\(03\)00134-1](https://doi.org/10.1016/S0012-821X(03)00134-1), 2003.
- Alcalá-Reygosa, J., Palacios, D., Schimmelpfennig, I., Vázquez-Selem, L., García-Sancho, L., Franco-Ramos, O., Villanueva, J., Zamorano, J. J., Aumaître, G., Bourlès, D., and Keddadouche, K.: Dating late Holocene lava flows in Pico de Orizaba (Mexico) by means of in situ-produced cosmogenic ^{36}Cl , lichenometry and dendrochronology, *Quaternary Geochronology*, 47, 93–106, <https://doi.org/10.1016/j.quageo.2018.05.011>, 2018.
- Anderson, S. W., Krinsley, D. H., and Fink, J. H.: Criteria for recognition of constructional silicic lava flow surfaces, *Earth Surface Processes and Landforms*, 19, 531–541, <https://doi.org/10.1002/esp.3290190606>, 1994.
- Balco, G., Stone, J. O., Lifton, N. A., and Dunai, T. J.: A complete and easily accessible means of calculating surface exposure ages or erosion rates from ^{10}Be and ^{26}Al measurements, *Quaternary Geochronology*, 3, 174–195, <https://doi.org/10.1016/j.quageo.2007.12.001>, 2008.
- Barrell, D. J.: Quaternary Glaciers of New Zealand, in: *Developments in Quaternary Sciences*, chap. 75, pp. 1047–1064, Elsevier, 15 edn., <https://doi.org/10.1016/B978-0-444-53447-7.00075-1>, 2011.
- Barrell, D. J. A., Almond, P. C., Vandergoes, M. J., Lowe, D. J., and Newnham, R. M.: A composite pollen-based stratotype for inter-regional evaluation of climatic events in New Zealand over the past 30,000 years (NZ-INTIMATE project), *Quaternary Science Reviews*, 74, 4–20, <https://doi.org/10.1016/j.quascirev.2013.04.002>, 2013.
- Blard, P.-H.: Cosmogenic ^3He in terrestrial rocks: A review, *Chemical Geology*, 586, 120–154, <https://doi.org/10.1016/j.chemgeo.2021.120543>, 2021.
- Blard, P.-H. and Farley, K. A.: The influence of radiogenic ^4He on cosmogenic ^3He determinations in volcanic olivine and pyroxene, *Earth and Planetary Science Letters*, 276, 20–29, <https://doi.org/10.1016/j.epsl.2008.09.003>, 2008.
- Blard, P. H., Pik, R., Lavé, J., Bourlès, D., Burnard, P. G., Yokochi, R., Marty, B., and Trusdell, F.: Cosmogenic ^3He production rates revisited from evidences of grain size dependent release of matrix-sited helium, *Earth and Planetary Science Letters*, 247, 222–234, <https://doi.org/10.1016/j.epsl.2006.05.012>, 2006.
- Blard, P. H., Lavé, J., Pik, R., Wagnon, P., and Bourlès, D.: Persistence of full glacial conditions in the central Pacific until 15,000 years ago, *Nature*, 449, 591–594, <https://doi.org/10.1038/nature06142>, 2007.
- Blard, P.-H., Braucher, R., Lavé, J., and Bourlès, D.: Cosmogenic ^{10}Be production rate calibrated against ^3He in the high Tropical Andes (3800–4900 m, 20°S), *Earth and Planetary Science Letters*, 382, 140–149, <https://doi.org/10.1016/j.epsl.2013.09.010>, 2013.
- Blard, P.-H., Balco, G., Burnard, P. G., Farley, K. A., Fenton, C. R., Friedrich, R., Jull, A. J., Niedermann, S., Pik, R., Schaefer, J. M., Scott, E. M., Shuster, D. L., Stuart, F. M., Stute, M., Tibari, B., Winckler, G., and Zimmermann, L.: An inter-laboratory comparison of cosmogenic ^3He and radiogenic ^4He in the CRONUS-P pyroxene standard, *Quaternary Geochronology*, 26, 11–19, <https://doi.org/10.1016/j.quageo.2014.08.004>, 2015.
- Bromley, G. R., Winckler, G., Schaefer, J. M., Kaplan, M. R., Licht, K. J., and Hall, B. L.: Pyroxene separation by HF leaching and its impact on helium surface-exposure dating, *Quaternary Geochronology*, 23, 1–8, <https://doi.org/10.1016/j.quageo.2014.04.003>, 2014.
- Buchanan-Banks, J. M., Lockwood, J. P., and Rubin, M.: Radiocarbon dates for lava flows from northeast rift zone of Mauna Loa volcano, Hilo $7\frac{1}{2}^\circ$ Quadrangle, island of Hawaii, *Radiocarbon*, 31, 179–186, 1989.

- 710 Calvert, A. T. and Lanphere, M. A.: Argon geochronology of Kilauea's early submarine history, *Journal of Volcanology and Geothermal Research*, 151, 1–18, <https://doi.org/10.1016/j.jvolgeores.2005.07.023>, 2006.
- Calvert, A. T., Fierstein, J., and Hildreth, W.: Eruptive history of Middle Sister, Oregon Cascades, USA-Product of a late Pleistocene eruptive episode, *Geosphere*, 14, 2118–2139, <https://doi.org/10.1130/GES01638.1>, 2018.
- Carignan, J., Hild, P., Mevelle, G., Morel, J., and Yeghicheyan, D.: Routine analyses of trace elements in geological samples using flow
715 injection and low pressure on-line liquid chromatography coupled to ICP-MS: A study of geochemical reference materials BR, DR-N, UB-N, AN-G and GH, *Geostandards Newsletter*, 25, 187–198, <https://doi.org/10.1111/j.1751-908x.2001.tb00595.x>, 2001.
- Cerling, T. E. and Craig, H.: Geomorphology and in-situ cosmogenic isotopes, *Annual Review of Earth and Planetary Sciences*, pp. 273–317, 1994.
- Clay, P. L., Busemann, H., Sherlock, S. C., Barry, T. L., Kelley, S. P., and McGarvie, D. W.: 40Ar/39Ar ages and residual
720 volatile contents in degassed subaerial and subglacial glassy volcanic rocks from Iceland, *Chemical Geology*, 403, 99–110, <https://doi.org/10.1016/j.chemgeo.2015.02.041>, 2015.
- Coble, M. A., Grove, M., and Calvert, A. T.: Calibration of Nu-Instruments Noblesse multicollector mass spectrometers for argon isotopic measurements using a newly developed reference gas, *Chemical Geology*, 290, 75–87, <https://doi.org/10.1016/j.chemgeo.2011.09.003>, 2011.
- 725 Cole, J. W. and Lewis, K. B.: Evolution of the Taupo-Hikurangi subduction system, *Tectonophysics*, 72, 1–21, [https://doi.org/10.1016/0040-1951\(81\)90084-6](https://doi.org/10.1016/0040-1951(81)90084-6), 1981.
- Connor, C., Bebbington, M., and Marzocchi, W.: Probabilistic Volcanic Hazard Assessment, Elsevier Inc., second edn., <https://doi.org/10.1016/b978-0-12-385938-9.00051-1>, 2015.
- Conway, C. E.: Studies on the Glaciovolcanic and Magmatic Evolution of Ruapehu Volcano, New Zealand, Phd thesis, Victoria University
730 of Wellington, <https://researcharchive.vuw.ac.nz/handle/10063/5152>, 2016.
- Conway, C. E., Townsend, D. B., Leonard, G. S., Wilson, C. J., Calvert, A. T., and Gamble, J. A.: Lava-ice interaction on a large composite volcano: a case study from Ruapehu, New Zealand, *Bulletin of Volcanology*, 77, <https://doi.org/10.1007/s00445-015-0906-2>, 2015.
- Conway, C. E., Leonard, G. S., Townsend, D. B., Calvert, A. T., Wilson, C. J., Gamble, J. A., Eaves, S. R., Pure, L. R., Leonard, G. S., Townsend, D. B., Wilson, C. J., Calvert, A. T., Cole, R. P., Conway, C. E., Gamble, J. A., and Smith, T. B.: A high-resolution 40Ar/39Ar
735 lava chronology and edifice construction history for Ruapehu volcano, New Zealand, *Journal of Volcanology and Geothermal Research*, 327, 152–179, <https://doi.org/10.1016/j.jvolgeores.2016.07.006>, 2016.
- Delunel, R., Blard, P.-H., Martin, L. C., Nomade, S., and Schlunegger, F.: Long term low latitude and high elevation cosmogenic 3He production rate inferred from a 107 ka-old lava flow in northern Chile; 22°S-3400 m a.s.l., *Geochimica et Cosmochimica Acta*, 184, 71–87, <https://doi.org/10.1016/j.gca.2016.04.023>, 2016.
- 740 Donoghue, S. L.: Late quaternary volcanic stratigraphy of the southeastern sector of the Mount Ruapehu ring plain New Zealand, Ph.D. thesis, Massey University, <https://mro.massey.ac.nz/items/516a0d80-eda3-4a7e-a495-2e13fcb7821c>, 1991.
- Donoghue, S. L. and Neall, V. E.: Late Quaternary constructional history of the southeastern Ruapehu ring plain, New Zealand, *New Zealand Journal of Geology and Geophysics*, 44, 439–466, <https://doi.org/10.1080/00288306.2001.9514949>, 2001.
- Donoghue, S. L., Neall, V. E., and Palmer, A. S.: Stratigraphy and chronology of late quaternary andesitic tephra deposits, Tongariro Volcanic
745 Centre, New Zealand, *Journal of the Royal Society of New Zealand*, 25, 115–206, <https://doi.org/10.1080/03014223.1995.9517487>, 1995.

- Donoghue, S. L., Stewart, R. B., Neall, V. E., Lecointre, J., Price, R., Palmer, A. S., McClelland, E., and Hobson, K.: The Tau-rewa Eruptive Episode: Evidence for climactic eruptions at Ruapehu volcano, New Zealand, *Bulletin of Volcanology*, 61, 223–240, <https://doi.org/https://doi.org/10.1007/s004450050273>, 1999.
- Donoghue, S. L., Vallance, J. W., Smith, I. E., and Stewart, R. B.: Using geochemistry as a tool for correlating proximal andesitic tephra : case studies from Mt Rainier (USA) and MT Ruapehu (New Zealand), *Journal of Quaternary Science*, 22, 395–410, <https://doi.org/10.1002/jqs.2007>, 2007.
- Dostal, J., Dupuy, C., Carron, J. P., Le Guen de Kerneizon, M., and Maury, R. C.: Partition coefficients of trace elements: Application to volcanic rocks of St. Vincent, West Indies, *Geochimica et Cosmochimica Acta*, 47, 525–533, [https://doi.org/10.1016/0016-7037\(83\)90275-2](https://doi.org/10.1016/0016-7037(83)90275-2), 1983.
- Dunai, T. J.: *Cosmogenic Nuclides. Principles, Concepts and Application in the Earth Surface Sciences*, Cambridge University Press, 2010.
- Dunn, T. and Sen, C.: Mineral/matrix partition coefficients for orthopyroxene, plagioclase, and olivine in basaltic to andesitic systems: A combined analytical and experimental study, *Geochimica et Cosmochimica Acta*, 58, 717–733, [https://doi.org/10.1016/0016-7037\(94\)90501-0](https://doi.org/10.1016/0016-7037(94)90501-0), 1994.
- Eaves, S. R. and Brook, M. S.: Glaciers and glaciation of North Island, New Zealand, *New Zealand Journal of Geology and Geophysics*, 64, 1–20, <https://doi.org/10.1080/00288306.2020.1811354>, 2021.
- Eaves, S. R., Winckler, G., Schaefer, J. J. M., Vandergoes, M. J., Alloway, B. V., Mackintosh, A. N., Townsend, D. B., Ryan, M. T., and Li, X.: A test of the cosmogenic ^3He production rate in the south-west Pacific (39°S), *Journal of Quaternary Science*, 30, 79–87, <https://doi.org/10.1002/jqs.2760>, 2015.
- Eaves, S. R., Mackintosh, A. N., Anderson, B. M., Doughty, A. M., Townsend, D. B., Conway, C. E., Winckler, G., Schaefer, J. M., Leonard, G. S., and Calvert, A. T.: The Last Glacial Maximum in the central North Island, New Zealand: Palaeoclimate inferences from glacier modelling, *Climate of the Past*, 12, 943–960, <https://doi.org/10.5194/cp-12-943-2016>, 2016a.
- Eaves, S. R., Mackintosh, A. N., Winckler, G., Schaefer, J. M., Alloway, B. V., and Townsend, D. B.: A cosmogenic ^3He chronology of late Quaternary glacier fluctuations in North Island, New Zealand (39°S), *Quaternary Science Reviews*, 132, 40–56, <https://doi.org/10.1016/j.quascirev.2015.11.004>, 2016b.
- Eaves, S. R., Winckler, G., Mackintosh, A. N., Schaefer, J. M., Townsend, D. B., Doughty, A. M., Jones, R. S., and Leonard, G. S.: Late-glacial and Holocene glacier fluctuations in North Island, New Zealand, *Quaternary Science Reviews*, 223, 105914, <https://doi.org/10.1016/j.quascirev.2019.105914>, 2019.
- Espanon, V. R., Honda, M., and Chivas, A. R.: Cosmogenic ^3He and ^{21}Ne surface exposure dating of young basalts from Southern Mendoza, Argentina, *Quaternary Geochronology*, 19, 76–86, <https://doi.org/10.1016/j.quageo.2013.09.002>, 2014.
- Fenton, C. R. and Niedermann, S.: Surface exposure dating of young basalts (1–200ka) in the San Francisco volcanic field (Arizona, USA) using cosmogenic ^3He and ^{21}Ne , *Quaternary Geochronology*, 19, 87–105, <https://doi.org/10.1016/j.quageo.2012.10.003>, 2014.
- Fenton, C. R., Webb, R. H., Pearthree, P. A., Cerling, T. E., and Poreda, R. J.: Displacement rates on the Toroweap and Hurricane faults: Implications for Quaternary downcutting in the Grand Canyon, Arizona, *Geology*, 29, 1035–1038, [https://doi.org/10.1130/0091-7613\(2001\)029<1035:DROTTA>2.0.CO;2](https://doi.org/10.1130/0091-7613(2001)029<1035:DROTTA>2.0.CO;2), 2001.
- Fenton, C. R., Niedermann, S., Goethals, M. M., Schneider, B., and Wijbrans, J.: Evaluation of cosmogenic ^3He and ^{21}Ne production rates in olivine and pyroxene from two Pleistocene basalt flows, western Grand Canyon, AZ, USA, *Quaternary Geochronology*, 4, 475–492, <https://doi.org/10.1016/j.quageo.2009.08.002>, 2009.

- 785 Ferrier, K. L., Taylor Perron, J., Mukhopadhyay, S., Rosener, M., Stock, J. D., Huppert, K. L., and Slosberg, M.: Covariation of climate and long-term erosion rates across a steep rainfall gradient on the Hawaiian island of Kaua'i, *Bulletin of the Geological Society of America*, 125, 1146–1163, <https://doi.org/10.1130/B30726.1>, 2013.
- Fierstein, J., Hildreth, W., and Calvert, A. T.: Eruptive history of South Sister, Oregon Cascades, *Journal of Volcanology and Geothermal Research*, 207, 145–179, <https://doi.org/10.1016/j.jvolgeores.2011.06.003>, 2011.
- Fleck, R. J., Hagstrum, J. T., Calvert, A. T., Evarts, R. C., and Conrey, R. M.: 40Ar/39Ar geochronology, paleomagnetism, and evolution of the Boring volcanic field, Oregon and Washington, USA, *Geosphere*, pp. 1283–1314, <https://doi.org/10.1130/GES00985.1>, 2014.
- 790 Foeken, J. P., Day, S., and Stuart, F. M.: Cosmogenic 3He exposure dating of the Quaternary basalts from Fogo, Cape Verdes: Implications for rift zone and magmatic reorganisation, *Quaternary Geochronology*, 4, 37–49, <https://doi.org/10.1016/j.quageo.2008.07.002>, 2009.
- Gabrielsen, H., Procter, J., Rainforth, H., Black, T., Harmsworth, G., and Pardo, N.: Reflections from an Indigenous Community on Volcanic Event Management, Communications and Resilience, *Advances in Volcanology*, pp. 463–479, https://doi.org/10.1007/11157_2016_44, 2018.
- 795 Gallahan, W. E. and Nielsen, R. L.: The partitioning of Sc, Y, and the rare earth elements between high-Ca pyroxene and natural mafic to intermediate lavas at 1 atmosphere, *Geochimica et Cosmochimica Acta*, 56, 2387–2404, [https://doi.org/10.1016/0016-7037\(92\)90196-P](https://doi.org/10.1016/0016-7037(92)90196-P), 1992.
- Gamble, J. A., Price, R. C., Smith, I. E., McIntosh, W. C., and Dunbar, N. W.: 40Ar/39Ar geochronology of magmatic activity, magma flux and hazards at Ruapehu volcano, Taupo Volcanic Zone, New Zealand, *Journal of Volcanology and Geothermal Research*, 120, 271–287, [https://doi.org/10.1016/S0377-0273\(02\)00407-9](https://doi.org/10.1016/S0377-0273(02)00407-9), 2003.
- 800 Gosse, J. C. and Phillips, F. M.: Terrestrial in situ cosmogenic nuclides: Theory and application, *Quaternary Science Reviews*, 20, 1475–1560, [https://doi.org/10.1016/S0277-3791\(00\)00171-2](https://doi.org/10.1016/S0277-3791(00)00171-2), 2001.
- Greve, A., Turner, G. M., Conway, C. E., Townsend, D. B., Gamble, J. A., and Leonard, G. S.: Palaeomagnetic refinement of the eruption ages of Holocene lava flows, and implications for the eruptive history of the Tongariro Volcanic Centre, New Zealand, *Geophysical Journal International*, 207, 702–718, <https://doi.org/10.1093/gji/ggw296>, 2016.
- 805 Hackett, W. R.: Geology and petrology of Ruapehu volcano and related vents, Phd thesis, Victoria University of Wellington, <http://researcharchive.vuw.ac.nz/handle/10063/743>, 1985.
- Harpel, C. J., Kyle, P. R., Esser, R. P., McIntosh, W. C., and Caldwell, D. A.: 40Ar/39Ar dating of the eruptive history of Mount Erebus, Antarctica: Summit flows, tephra, and caldera collapse, *Bulletin of Volcanology*, 66, 687–702, <https://doi.org/10.1007/s00445-004-0349-7>, 2004.
- 810 Harris, A. J. L.: Basaltic Lava Flow Hazard, in: *Volcanic Hazards, Risks and Disasters*, edited by Shroder, J. F. and Papale, P., chap. 2, pp. 17–46, Elsevier, <https://doi.org/10.1016/C2011-0-07012-6>, 2015.
- Hilton, D. R., Fischer, T. P., and Marry, B.: Noble gases and volatile recycling at subduction zones, *Reviews in Mineralogy and Geochemistry*, 47, <https://doi.org/10.2138/rmg.2002.47.9>, 2002.
- 815 Houghton, B. F., Wilson, C. J., McWilliams, M. O., Lanphere, M. A., Weaver, S. D., Briggs, R. M., and Pringle, M. S.: Chronology and dynamics of a large silicic magmatic system: central Taupo Volcanic Zone, New Zealand, *Geology*, 23, 13–16, [https://doi.org/10.1130/0091-7613\(1995\)023<0013:CADOAL>2.3.CO;2](https://doi.org/10.1130/0091-7613(1995)023<0013:CADOAL>2.3.CO;2), 1995.
- Jenkins, S. F., Day, S. J., Faria, B. V., and Fonseca, J. F.: Damage from lava flows: insights from the 2014–2015 eruption of Fogo, Cape Verde, *Journal of Applied Volcanology*, 6, <https://doi.org/10.1186/s13617-017-0057-6>, 2017.

- 820 Keys, H. and Green, P. M.: Mitigation of volcanic risks at Mt Ruapehu, New Zealand, Proceedings of the Mountain Risks international conference, Firenze, Italy, pp. 485–490, 2010.
- Klein, J., Giegengack, R., Middleton, R., Sharma, P., Underwood, J. R., and Weeks, R. A.: Revealing Histories of Exposure Using in Situ Produced ^{26}Al and ^{10}Be in Libyan Desert Glass, *Radiocarbon*, 28, 547–555, 1986.
- Kurz, M. D.: Cosmogenic helium in a terrestrial igneous rock, *Nature*, 320, 435–439, <https://doi.org/10.1038/320435a0>, 1986a.
- 825 Kurz, M. D.: In situ production of terrestrial cosmogenic helium and some applications to geochronology, *Geochimica et Cosmochimica Acta*, 50, 2855–2862, [https://doi.org/10.1016/0016-7037\(86\)90232-2](https://doi.org/10.1016/0016-7037(86)90232-2), 1986b.
- Kurz, M. D., Colodner, D., Trull, T. W., Moore, R. B., and O'Brien, K.: Cosmic ray exposure dating with in situ produced cosmogenic ^3He : results from young Hawaiian lava flows, *Earth and Planetary Science Letters*, 97, 177–189, [https://doi.org/10.1016/0012-821X\(90\)90107-9](https://doi.org/10.1016/0012-821X(90)90107-9), 1990.
- 830 Lal, D.: An important source of ^4He (and ^3He) in diamonds, *Earth and Planetary Science Letters*, 96, 1–7, [https://doi.org/10.1016/0012-821X\(89\)90118-0](https://doi.org/10.1016/0012-821X(89)90118-0), 1989.
- Lal, D.: Cosmic ray labeling of erosion surfaces: in situ nuclide production rates and erosion models, *Earth and Planetary Science Letters*, 104, 424–439, [https://doi.org/https://doi.org/10.1016/0012-821X\(91\)90220-C](https://doi.org/https://doi.org/10.1016/0012-821X(91)90220-C), 1991.
- Lanphere, M. A.: Comparison of conventional K-Ar and $^{40}\text{Ar}/^{39}\text{Ar}$ dating of young mafic volcanic rocks, *Quaternary Research*, 53, 294–301, <https://doi.org/10.1006/qres.1999.2122>, 2000.
- 835 Le Maitre, R. W.: *Igneous Rocks: A Classification and Glossary of Terms, Recommendations of the International Union of Geological Sciences, Subcommission of the Systematics of Igneous Rocks*, Cambridge University Press, 2002.
- Leonard, G. S., Cole, R. P. R., Christenson, B. W., Conway, C. E., Cronin, S. J., Gamble, J. A., Hurst, T., Kennedy, B. M., Miller, C. A., Procter, J. N., Pure, L. R., Townsend, D. B., White, J. D., and Wilson, C. J.: Ruapehu and Tongariro stratovolcanoes: a review of current understanding, *New Zealand Journal of Geology and Geophysics*, 64, 389–420, <https://doi.org/10.1080/00288306.2021.1909080>, 2021.
- 840 Leya, I., Lange, H. J., Neumann, S., Wieler, R., and Michel, R.: The production of cosmogenic nuclides in stony meteoroids by galactic cosmic-ray particles, *Meteoritics and Planetary Science*, 35, 259–286, <https://doi.org/10.1111/j.1945-5100.2001.tb01845.x>, 2000.
- Licciardi, J. M., Kurz, M. D., and Curtice, J. M.: Cosmogenic ^3He production rates from Holocene lava flows in Iceland, *Earth and Planetary Science Letters*, 246, 251–264, <https://doi.org/10.1016/j.epsl.2006.03.016>, 2006.
- 845 Licciardi, J. M., Kurz, M. D., and Curtice, J. M.: Glacial and volcanic history of Icelandic table mountains from cosmogenic ^3He exposure ages, *Quaternary Science Reviews*, 26, 1529–1546, <https://doi.org/10.1016/j.quascirev.2007.02.016>, 2007.
- Lifton, N.: Implications of two Holocene time-dependent geomagnetic models for cosmogenic nuclide production rate scaling, *Earth and Planetary Science Letters*, 433, 257–268, <https://doi.org/10.1016/j.epsl.2015.11.006>, 2016.
- Lifton, N., Sato, T., and Dunai, T. J.: Scaling in situ cosmogenic nuclide production rates using analytical approximations to atmospheric cosmic-ray fluxes, *Earth and Planetary Science Letters*, 386, 149–160, <https://doi.org/10.1016/j.epsl.2013.10.052>, 2014.
- 850 Lippolt, H. J. and Weigel, E.: ^4He diffusion in ^{40}Ar -retentive minerals, *Geochimica et Cosmochimica Acta*, 52, 1449–1458, [https://doi.org/10.1016/0016-7037\(88\)90215-3](https://doi.org/10.1016/0016-7037(88)90215-3), 1988.
- Lockwood, J. P. and Lipman, P. W.: Recovery of datable charcoal beneath young lavas: Lessons from Hawaii, *Bulletin Volcanologique*, 43, 609–615, <https://doi.org/10.1007/BF02597697>, 1980.
- 855 Luhr, J. F. and Carmichael, I. S. E.: The Colima Volcanic complex, Mexico, *Contributions to Mineralogy and Petrology*, 71, 343–372, <https://doi.org/10.1007/bf00374707>, 1980.

- Lupton, J. and Evans, L.: Changes in the atmospheric helium isotope ratio over the past 40 years, *Geophysical Research Letters*, 40, 6271–6275, <https://doi.org/10.1002/2013GL057681>, 2013.
- Marchetti, D. W., Hynke, S. A., and Cerling, T. E.: Cosmogenic ^3He exposure ages of basalt flows in the northwestern Payún Matru volcanic field, Mendoza Province, Argentina, *Quaternary Geochronology*, 19, 67–75, <https://doi.org/10.1016/j.quageo.2012.10.004>, 2014.
- Martin, L. C., Blard, P.-H., Balco, G., Lavé, J., Delunel, R., Lifton, N., and Laurent, V.: The CREP program and the ICE-D production rate calibration database: A fully parameterizable and updated online tool to compute cosmic-ray exposure ages, *Quaternary Geochronology*, 38, 25–49, <https://doi.org/10.1016/j.quageo.2016.11.006>, 2017.
- Matsuda, J., Matsumoto, T., Sumino, H., Nagao, K., Yamamoto, J., Miura, Y., Kaneoka, I., Takahata, N., and Sano, Y.: The $^3\text{He}/^4\text{He}$ ratio of new internal He Standard of Japan (HESJ), *Geochemical Journal*, 36, 191–195, <https://doi.org/10.2343/geochemj.36.191>, 2002.
- Mc Arthur, J. L. and Shepherd, M. J.: Late Quaternary glaciation of Mt. Ruapehu, North Island, New Zealand, *Journal of the Royal Society of New Zealand*, 20, 287–296, <https://doi.org/10.1080/03036758.1990.10416823>, 1990.
- Medynski, S., Pik, R., Burnard, P., Vye-Brown, C., France, L., Schimmelpfennig, I., Whaler, K., Johnson, N., Benedetti, L., Ayelew, D., and Yirgu, G.: Stability of rift axis magma reservoirs: Spatial and temporal evolution of magma supply in the Dabbahu rift segment (Afar, Ethiopia) over the past 30 kyr, *Earth and Planetary Science Letters*, 409, 278–289, <https://doi.org/10.1016/j.epsl.2014.11.002>, 2015.
- Mishra, A. K., Placzek, C., Wurster, C., and Whitehead, P. W.: New radiocarbon age constraints for the 120 km-long Toomba flow, north Queensland, Australia, *Australian Journal of Earth Sciences*, 66, 71–79, <https://doi.org/10.1080/08120099.2019.1523227>, 2019.
- Moore, R. B. and Rubin, M.: Radiocarbon dates for lava flows and pyroclastic deposits on Sao Miguel, Azores, *Radiocarbon*, 33, 151–164, <https://doi.org/10.1017/S0033822200013278>, 1991.
- Morimoto, N., Fabries, J., Ferguson, A., Ginzburg, I., Ross, M., Seifert, F., Zussman, J., Aoki, K., and Gottardi, G.: Nomenclature of pyroxenes Subcommittee on Pyroxenes Commission on New Minerals and Mineral Names International Mineralogical Association, *American Mineralogist*, 73, 1123–1133, 1988.
- Muscheler, R., Beer, J., Kubik, P. W., and Synal, H. A.: Geomagnetic field intensity during the last 60,000 years based on ^{10}Be and ^{36}Cl from the Summit ice cores and ^{14}C , *Quaternary Science Reviews*, 24, 1849–1860, <https://doi.org/10.1016/j.quascirev.2005.01.012>, 2005.
- Nairn, I. A., Kobayashi, T., and Nakagawa, M.: The ~ 10 ka multiple vent pyroclastic eruption sequence at Tongariro Volcanic Centre, Taupo Volcanic Zone, New Zealand: Part 1. Eruptive processes during regional extension, *Journal of Volcanology and Geothermal Research*, 86, 19–44, [https://doi.org/10.1016/S0377-0273\(98\)00085-7](https://doi.org/10.1016/S0377-0273(98)00085-7), 1998.
- Nicholls, I. A. and Harris, K. L.: Experimental rare earth element partition coefficients for garnet, clinopyroxene and amphibole coexisting with andesitic and basaltic liquids, *Geochimica et Cosmochimica Acta*, 44, 287–308, [https://doi.org/10.1016/0016-7037\(80\)90138-6](https://doi.org/10.1016/0016-7037(80)90138-6), 1980.
- Niedermann, S.: Cosmic-ray-produced noble gases in terrestrial rocks: Dating tools for surface processes, *Reviews in Mineralogy and Geochemistry*, 47, <https://doi.org/10.2138/rmg.2002.47.16>, 2002.
- Nishiizumi, K.: Cosmic ray production rates of ^{10}Be and ^{26}Al in quartz from glacially polished rocks, *Journal of Geophysical Research*, 94, <https://doi.org/10.1029/jb094ib12p17907>, 1989.
- Nishiizumi, K., Kohl, C. P., Arnold, J. R., Klein, J., Fink, D., and Middleton, R.: Cosmic ray produced ^{10}Be and ^{26}Al in Antarctic rocks: exposure and erosion history, *Earth and Planetary Science Letters*, 104, 440–454, [https://doi.org/10.1016/0012-821X\(91\)90221-3](https://doi.org/10.1016/0012-821X(91)90221-3), 1991.
- Palmer, B. A. and Neall, V. E.: The Murimotu Formation—9500 year old deposits of a debris avalanche and associated lahars, Mount Ruapehu, North Island, New Zealand, *New Zealand Journal of Geology and Geophysics*, 32, 477–486, <https://doi.org/10.1080/00288306.1989.10427555>, 1989.

- 895 Pardo, N.: Andesitic Plinian Eruptions at Mt. Ruapehu (New Zealand): From Lithofacies to Eruption Dynamics, Phd thesis, Massey University, <https://mro.massey.ac.nz/items/c2f61b33-2579-410f-b493-eeab08691375>, 2012.
- Pardo, N., Cronin, S., Palmer, A., Procter, J., and Smith, I.: Andesitic Plinian eruptions at Mt. Ruapehu: Quantifying the uppermost limits of eruptive parameters, *Bulletin of Volcanology*, 74, 1161–1185, <https://doi.org/10.1007/s00445-012-0588-y>, 2012a.
- Pardo, N., Cronin, S. J., Palmer, A. S., and Németh, K.: Reconstructing the largest explosive eruptions of Mt. Ruapehu, New Zealand: Lithostratigraphic tools to understand subplinian-plinian eruptions at andesitic volcanoes, *Bulletin of Volcanology*, 74, 617–640, <https://doi.org/10.1007/s00445-011-0555-z>, 2012b.
- 900 Parmelee, D. E., Kyle, P. R., Kurz, M. D., Marrero, S. M., and Phillips, F. M.: A new Holocene eruptive history of Erebus volcano, Antarctica using cosmogenic ^3He and ^{36}Cl exposure ages, *Quaternary Geochronology*, 30, 114–131, <https://doi.org/10.1016/j.quageo.2015.09.001>, 2015.
- 905 Patterson, D. B., Honda, M., and McDougall, I.: Noble gases in mafic phenocrysts and xenoliths from New Zealand, *Geochimica et Cosmochimica Acta*, 58, 4411–4427, [https://doi.org/10.1016/0016-7037\(94\)90344-1](https://doi.org/10.1016/0016-7037(94)90344-1), 1994.
- Preece, K., Mark, D. F., Barclay, J., Cohen, B. E., Chamberlain, K. J., Jowitt, C., Vye-Brown, C., Brown, R. J., and Hamilton, S.: Bridging the gap: $^{40}\text{Ar}/^{39}\text{Ar}$ dating of volcanic eruptions from the 'Age of Discovery', *Geology*, 46, 1035–1038, <https://doi.org/10.1130/G45415.1>, 2018.
- 910 Price, R. C., Gamble, J. A., Smith, I. E., Maas, R., Waight, T., Stewart, R. B., and Woodhead, J.: The anatomy of an andesite volcano: A time-stratigraphic study of andesite petrogenesis and crustal evolution at Ruapehu Volcano, New Zealand, *Journal of Petrology*, 53, 2139–2189, <https://doi.org/10.1093/petrology/egs050>, 2012.
- Puchol, N., Blard, P.-H., Pik, R., Tibari, B., and Lavé, J.: Variability of magmatic and cosmogenic ^3He in Ethiopian river sands of detrital pyroxenes: Impact on denudation rate determinations, *Chemical Geology*, 448, 13–25, <https://doi.org/10.1016/j.chemgeo.2016.10.033>, 2017.
- 915 Pure, L. R., Leonard, G. S., Townsend, D. B., Wilson, C. J., Calvert, A. T., Cole, R. P., Conway, C. E., Gamble, J. A., and Smith, T. B.: A high resolution $^{40}\text{Ar}/^{39}\text{Ar}$ lava chronology and edifice construction history for Tongariro volcano, New Zealand, *Journal of Volcanology and Geothermal Research*, 403, 106993, <https://doi.org/10.1016/j.jvolgeores.2020.106993>, 2020.
- Ramos, F. C., Heizler, M. T., Buettner, J. E., Gill, J. B., Wei, H. Q., Dimond, C. A., and Scott, S. R.: U-series and $^{40}\text{Ar}/^{39}\text{Ar}$ ages of Holocene volcanic rocks at Changbaishan volcano, China, *Geology*, 44, 511–514, <https://doi.org/10.1130/G37837.1>, 2016.
- 920 Rhodes, E.: The Draining of an Andesitic Valley-Confined Lava Flow, Mt Ruapehu, Honours thesis, University of Canterbury, 2012.
- Schaefer, J. M., Winckler, G., Blard, P.-H., Balco, G., Shuster, D. L., Friedrich, R., Jull, A. J. T., Wieler, R., and Schluechter, C.: Performance of CRONUS-P - A pyroxene reference material for helium isotope analysis, *Quaternary Geochronology*, 31, 237–239, <https://doi.org/10.1016/j.quageo.2014.07.006>, 2016.
- 925 Schimmelpfennig, I., Williams, A., Pik, R., Burnard, P., Niedermann, S., Finkel, R., Schneider, B., and Benedetti, L.: Inter-comparison of cosmogenic in-situ ^3He , ^{21}Ne and ^{36}Cl at low latitude along an altitude transect on the SE slope of Kilimanjaro volcano (3°S , Tanzania), *Quaternary Geochronology*, 6, 425–436, <https://doi.org/10.1016/j.quageo.2011.05.002>, 2011.
- Sherrod, D. R., Hagstrum, J. T., Mcgeehin, J. P., Champion, D. E., and Trusdell, F. A.: Distribution, ^{14}C chronology, and paleomagnetism of latest Pleistocene and Holocene lava flows at Haleakala Island of Maui, Hawaii: A revision of lava flow hazard zones, *Journal of Geophysical Research*, 111, <https://doi.org/10.1029/2005JB003876>, 2006.
- 930

- Shuster, D. L., Farley, K. A., Sisterson, J. M., and Burnett, D. S.: Quantifying the diffusion kinetics and spatial distributions of radiogenic ^4He in minerals containing proton-induced ^3He , *Earth and Planetary Science Letters*, 217, 19–32, [https://doi.org/10.1016/S0012-821X\(03\)00594-6](https://doi.org/10.1016/S0012-821X(03)00594-6), 2004.
- Smith, J. A., Finkel, R. C., Farber, D. L., Rodbell, D. T., and Seltzer, G. O.: Moraine preservation and boulder erosion in the tropical Andes: Interpreting old surface exposure ages in glaciated valleys, *Journal of Quaternary Science*, 20, 735–758, <https://doi.org/10.1002/jqs.981>, 2005.
- Stipp, J.: The Geochronology and Petrogenesis of the Cenozoic Volcanics of the North Island, New Zealand, Phd thesis, Australian National University, 1968.
- Stone, J. O.: Air pressure and cosmogenic isotope production, *Journal of Geophysical Research*, 105, 753–759, <https://doi.org/https://doi.org/10.1029/2000JB900181>, 2000.
- Tanaka, H., Kawamura, K., Nagao, K., and Houghton, B. F.: K-Ar ages and paleosecular variation of direction and intensity from quaternary lava sequences in the Ruapehu Volcano, New Zealand, *Earth, Planets and Space*, 49, 587–599, <https://doi.org/https://doi.org/10.5636/jgg.49.587>, 1997.
- Topping, W. W.: Some aspects of quaternary history of Tongariro Volcanic Centre, Phd thesis, Victoria University of Wellington, 1974.
- Topping, W. W. and Kohn, B. P.: Rhyolitic tephra marker beds in the Tongariro area, North Island, New Zealand, *New Zealand Journal of Geology and Geophysics*, 16, 375–395, <https://doi.org/10.1080/00288306.1973.10431367>, 1973.
- Townsend, D., Leonard, G., Conway, C., Eaves, S., and Wilson, C.: Geology of the Tongariro National Park Area, GNS Science, pp. 1 sheet + 109 pp, 2017.
- Tremblay, M. M., Shuster, D. L., and Balco, G.: Diffusion kinetics of ^3He and ^{21}Ne in quartz and implications for cosmogenic noble gas paleothermometry, *Geochimica et Cosmochimica Acta*, 142, 186–204, <https://doi.org/10.1016/j.gca.2014.08.010>, 2014.
- Trusdell, F. A.: Lava flow hazards and risk assessment on Mauna Loa Volcano, Hawaii, *Geophysical Monograph Series*, 92, 327–336, <https://doi.org/10.1029/GM092p0327>, 1995.
- Tsang, S. and Lindsay, J.: Lava flow crises in inhabited areas part I: Lessons learned and research gaps related to effusive, basaltic eruptions, *Journal of Applied Volcanology*, 9, 1–26, <https://doi.org/10.1186/s13617-020-00096-y>, 2020.
- Turner, G. M. and Corkill, R. M.: NZPSV11k.2023 and NZPSV1k.2023: Holocene palaeomagnetic secular variation master records for New Zealand, *Physics of the Earth and Planetary Interiors*, 344, 107 093, <https://doi.org/10.1016/j.pepi.2023.107093>, 2023.
- Turner, G. M., Howarth, J. D., de Gelder, G. I., and Fitzsimons, S. J.: A new high-resolution record of Holocene geomagnetic secular variation from New Zealand, *Earth and Planetary Science Letters*, 430, 296–307, <https://doi.org/10.1016/j.epsl.2015.08.021>, 2015.
- Uppala, S. M., Kållberg, P. W., Simmons, A. J., Andrae, U., da Costa Bechtold, V., Fiorino, M., Gibson, J. K., Haseler, J., Hernandez, A., Kelly, G. A., Li, X., Onogi, K., Saarinen, S., Sokka, N., Allan, R. P., Andersson, E., Arpe, K., Balmaseda, M. A., Beljaars, A. C., van de Berg, L., Bidlot, J., Bormann, N., Caires, S., Chevallier, F., Dethof, A., Dragosavac, M., Fisher, M., Fuentes, M., Hagemann, S., Hólm, E., Hoskins, B. J., Isaksen, I., Janssen, P. A., Jenne, R., McNally, A. P., Mahfouf, J. F., Morcrette, J. J., Rayner, N. A., Saunders, R. W., Simon, P., Sterl, A., Trenberth, K. E., Untch, A., Vasiljevic, D., Viterbo, P., and Woollen, J.: The ERA-40 re-analysis, *Quarterly Journal of the Royal Meteorological Society*, 131, 2961–3012, <https://doi.org/10.1256/qj.04.176>, 2005.
- Vermeesch, P.: IsoplotR: A free and open toolbox for geochronology, *Geoscience Frontiers*, 9, 1479–1493, <https://doi.org/10.1016/j.gsf.2018.04.001>, 2018.
- Villemant, B.: Trace element evolution in the Phlegrean Fields (Central Italy): fractional crystallization and selective enrichment, *Contributions to Mineralogy and Petrology*, 98, 169–183, <https://doi.org/10.1007/BF00402110>, 1988.

- Wijbrans, J., Schneider, B., Kuiper, K., Calvari, S., Branca, S., De Beni, E., Norini, G., Corsaro, R. A., and Miraglia,
970 L.: 40Ar/39Ar geochronology of Holocene basalts; examples from Stromboli, Italy, *Quaternary Geochronology*, 6, 223–232,
<https://doi.org/10.1016/j.quageo.2010.10.003>, 2011.
- Wilson, C. J., Gravley, D. M., Leonard, G. S., and Rowland, J. V.: Volcanism in the central Taupo Volcanic Zone, New Zealand: tempo, styles
and controls, in: *Studies in Volcanology: The Legacy of George Walker*, edited by Thordarson, T., pp. 225–247, Special Publications of
IAVCEI 2, 2009.
- 975 Wilson, G., Wilson, T. M., Deligne, N. I., and Cole, J. W.: Volcanic hazard impacts to critical infrastructure: A review, *Journal of Volcanology
and Geothermal Research*, 286, 148–182, <https://doi.org/10.1016/j.jvolgeores.2014.08.030>, 2014.
- Wright, H. M., Vazquez, J. A., Champion, D. E., Calvert, A. T., Mangan, M. T., Stelten, M., Cooper, K. M., Herzig, C., and Jr, A. S.: Episodic
Holocene eruption of the Salton Buttes rhyolites, California, from paleomagnetic, U-Th, and Ar/Ar dating Heather, *Geochemistry, Geo-
physics, Geosystems*, 16, 1198–1210, <https://doi.org/10.1002/2015GC005714>.Received, 2015.
- 980 Zimmermann, L., Avice, G., Blard, P.-H., Marty, B., Füre, E., and Burnard, P. G.: A new all-metal induction furnace for noble gas extraction,
Chemical Geology, 480, 86–92, <https://doi.org/10.1016/j.chemgeo.2017.09.018>, 2018.